J. Fluid Mech. (2008), *vol.* 607, *pp.* 313–350.
doi:10.1017/S0022112008002061 Printed in the United Kingdom

Modelling phase transition in metastable liquids: application to cavitating and flashing flows

RICHARD SAUREL[1,3]†, FABIEN PETITPAS[1] AND REMI ABGRALL[2,3]

[1]Polytech'Marseille, Aix-Marseille Université and SMASH Project UMR CNRS 6595 - IUSTI - INRIA, 5 rue E. Fermi, 13453 Marseille Cedex 13, France

[2]SCALAPPLIX Project, INRIA and Institut de Mathématiques, Université de Bordeaux I, 351 cours de la Libération, 33405 Talence Cedex, France

[3]University Institute of France

(Received 23 March 2007 and in revised form 18 April 2008)

A hyperbolic two-phase flow model involving five partial differential equations is constructed for liquid–gas interface modelling. The model is able to deal with interfaces of simple contact where normal velocity and pressure are continuous as well as transition fronts where heat and mass transfer occur, involving pressure and velocity jumps. These fronts correspond to extra waves in the system. The model involves two temperatures and entropies but a single pressure and a single velocity. The closure is achieved by two equations of state that reproduce the phase diagram when equilibrium is reached. Relaxation toward equilibrium is achieved by temperature and chemical potential relaxation terms whose kinetics is considered infinitely fast at specific locations only, typically at evaporation fronts. Thus, metastable states are involved for locations far from these fronts. Computational results are compared to the experimental ones. Computed and measured front speeds are of the same order of magnitude and the same tendency of increasing front speed with initial temperature is reported. Moreover, the limit case of evaporation fronts propagating in highly metastable liquids with the Chapman–Jouguet speed is recovered as an expansion wave of the present model in the limit of stiff thermal and chemical relaxation.

1. Introduction

When a liquid initially in thermodynamic equilibrium is subject to strong rarefaction waves, it may reach a metastable state where the temperature is higher than the saturated one at the final pressure of the expanded state. Then the superheated liquid releases its metastable energy (stored as internal energy) very quickly, even explosively, producing either pure vapour, if the liquid is retrograde (Chaves 1984; Thompson *et al.* 1987; Kurschat, Chaves & Meier 1992), or a liquid-vapour mixture at high velocity. This phenomenon is often called cavitation. Such situations appear frequently in nature and in many industrial applications, such as liquid flows around hypervelocity projectiles and submarine airfoils, or inside nozzles such as fuel injector systems. Cavitation in these systems always produces strong disturbances. In most applications, cavitation appears as a multi-dimensional phenomenon due to geometrical effects. This multi-dimensional character complicates both experiments and theoretical approaches.

† Author to whom correspondence should be addressed: richard.saurel@polytech.univ-mrs.fr

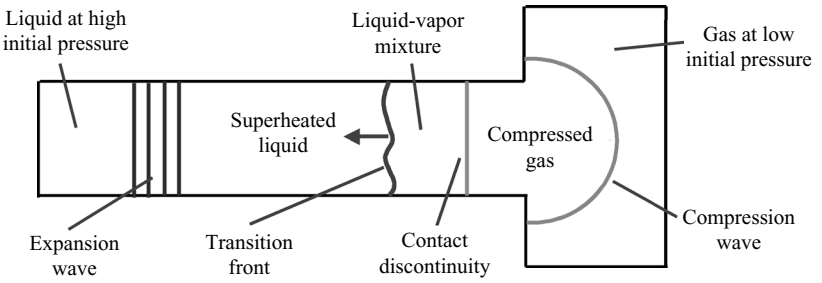

FIGURE 1. Simplified experimental setup of the expansion tube used by Simoes-Moreira & Shepherd (1999) and associated waves.

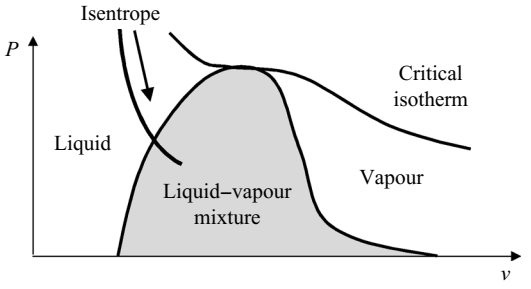

FIGURE 2. Liquid thermodynamic path associated to the expansion wave producing a superheated liquid.

By using one-dimensional expansion tubes several authors (Grolmes & Fauske 1974; Chaves 1984; Thompson *et al.* 1987; Hill & Sturtevant 1990; Frost, Lee & Ciccarelli 1991; Kurschat *et al.* 1992; Simoes-Moreira & Shepherd 1999; Reinke & Yadigaroglu 2001) have succeeded of isolating the main phenomenon that we propose to summarize hereafter. These experiments consisted of connecting a vertical tube filled with a liquid in thermodynamic equilibrium at atmospheric pressure (or higher) to a very low-pressure chamber (figure 1). As soon as the membrane between the liquid and the vacuum chamber is ruptured, rarefaction waves propagate through the liquid producing a superheated liquid (figure 2).

Then a subsonic phase-transition front propagates through the superheated liquid producing a high-velocity liquid-vapour mixture in thermodynamic equilibrium moving towards the low-pressure chamber. The front velocity is approximately $1\,\mathrm{m\,s^{-1}}$ while the ejected mixture velocity is of the order of $100\,\mathrm{m\,s^{-1}}$.

These experimental observations indicate that both liquid and vapour compressibilities have to be considered. They also report the presence of an acoustic wave (expansion wave) preceding the evaporation front, itself preceding a contact discontinuity and a compression wave as represented in the figure 1. The corresponding wave pattern is shown in the (x, t) diagram of figure 3. Expansion effects in industrial systems are often due to geometrical effects, for example in nozzles where cavitation appears at locations where the pressure is very low and the liquid superheated (figure 4).

The aim of the present paper is to develop a model able to deal with metastable states and evaporation front dynamics, as well as the other waves shown in figure 3. The model must also be able to deal with interfaces separating a liquid and a non-condensable gas; mass transfer occurs only under specific thermodynamic conditions that do not necessarily correspond to the local thermodynamic state at the interfaces.

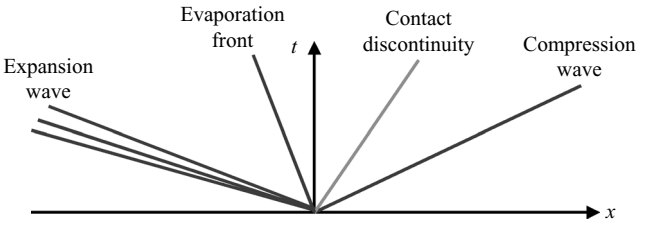

FIGURE 3. A typical wave pattern of cavitating systems.

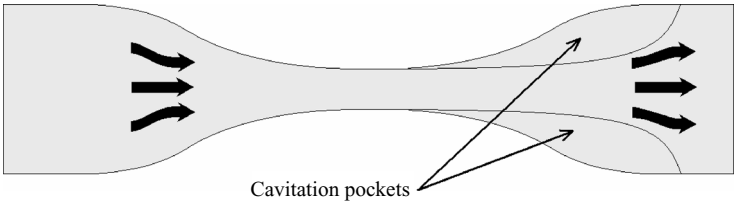

FIGURE 4. Cavitating flow in a nozzle. Cavitation pockets appear in the divergent part of the nozzle where geometrical expansion produces metastable liquid state.

Thus the model must be able to deal with interfaces of simple contact as well as evaporating interfaces.

The paper is organized as follows. Existing model are reviewed and a critical analysis is given in § 2, together with justification of the choice for temperature non-equilibrium model. In § 3, starting from the non-equilibrium model of Baer & Nunziato (1986) an asymptotic analysis is carried out in order to derive a single velocity and pressure two-phase flow model including heat transfers. This model can solve interface problems with non-miscible fluids. Its thermodynamic closure is examined in § 4. Mass transfer modelling is addressed in § 5. Closure relations are obtained by examining the entropy production in each phase and in the mixture. The basic ingredients needed to solve the hyperbolic system with heat and mass transfer are reported in § 6. Numerical results are reported in § 7. The limit case of interfaces separating pure non-miscible fluids is examined. Then mass transfer is introduced adding extra waves into the system. Computed results are compared to the experimental ones of Simoes-Moreira & Shepherd (1999). A new interpretation of evaporation front dynamics in highly metastable liquids (Chaves 1984) is proposed. Such fronts correspond to expansion waves of the limit system with stiff thermal and chemical relaxation.

2. Review of existing models

Essentially two classes of models are available in the literature. The first class corresponds to pressure and temperature equilibrium models, the second class being related to temperature non-equilibrium models.

2.1. *Pressure and temperature equilibrium models*

At least four models belong to this category, with increasing complexity:

(i) The mixture Euler equations with a cubic equation of state (EOS). A prototype of such an EOS is the van der Waals one. With such models a loss of hyperbolicity occurs in the spinodal region. In other words, the squared sound speed may become negative and wave propagation has no physical meaning (Menikoff & Plohr 1989).

(ii) The mixture Euler equations can also be used with a tabular EOS or a combination of pure phase EOSs with the assumption of pressure, temperature and chemical potential equilibrium in the two-phase region (see for example Saurel, Cocchi & Butler 1999; Liou & Edwards 1999). Such models remove the preceding loss of hyperbolicity. However, the mixture is assumed to evolve under thermodynamic equilibrium, thus there are no metastable states. Also, the model is unable to deal with material interfaces separating a liquid and a non-condensable gas. Hence, it has a restricted domain of application.

(iii) The mixture Euler equations are sometimes augmented by a mass fraction equation with a relaxation term (Faucher *et al.* 2000), as is frequently done for mixtures of reacting gases. This four-equation model is unable to solve interfaces between a liquid and a non-condensable gas (water/air for example) as its isothermal closure is not compatible with interface conditions (equal pressures and normal velocities but not temperatures). Moreover, determination of the mass relaxation term is a problem.

(iv) Models can be derived from the second-gradient theory (Cahn & Hilliard 1958). In this approach, the interface is described as a diffuse zone with a capillary length scale that has to be resolved. This results in severe restrictions as this zone length is typically of the order of one nanometre. To do practical simulations, at the scale of an individual bubble for example, the interface has to be thickened (Jamet *et al.* 2001). Such a procedure has important consequences for the model's ability to deal with metastable states. Also, interfaces with large density gradients are very difficult to solve, as are interfaces separating immiscible fluids (water/air for example).

2.2. *Temperature non-equilibrium models*

At least three models belong to this category:

(i) The most conventional temperature non-equilibrium model is the six-equation model obtained for example with averaging methods (Ishii 1975; Delhaye & Boure 1982). It involves a balance equation of mass, momentum and energy for each fluid. Unlike the preceeding models, the mixture evolves with two velocities. It is present in the literature with two options:

(*a*) One of the phases is considered incompressible, the mixture pressure being that of the gas phase. This is not compatible with the presence of rarefaction waves in the liquid phase, whose presence is mandatory in cavitating flows.

(*b*) Both phases are compressible and the closure is achieved with the pressure equilibrium assumption (Butler, Lambeck & Krier 1982).

The six-equation model, with both options, has a restricted domain of hyperbolicity. This results in a restricted validity for problems where transient wave propagation is not important. Moreover, it is unable to solve interface problems (water/air for example).

(ii) The seven-equation model (Baer & Nunziato 1986) (and its variants) is unconditionally hyperbolic and is able to deal with a wide range of applications. It is composed of the same six equations as previously, augmented by an evolution equation for the volume fraction of one of the constituents. Its ability to solve interface problems as well as fluid mixtures with several velocities was demonstrated in Saurel & Abgrall (1999), Saurel & Le Metayer (2001) and Saurel, Gavrilyuk & Renaud (2003). This model has been extended to the propagation of evaporation fronts in cavitating systems (Le Metayer, Massoni & Saurel 2005). The four waves present in figure 3 are correctly captured and the model is able to deal with metastable states. It has been used for practical computations and validated against experiments on

supercavitation. However it is quite complex to code and does not provide information about the structure of the evaporation front, as the front is considered as a sharp discontinuity.

(iii) The last model involves a single pressure and velocity. It is composed of two mass balance equations, one mixture momentum equation, one mixture energy equation and a volume fraction equation. This five-equation model (Kapila *et al.* 2001) is unconditionally hyperbolic. Its ability to solve interface problems with compressible fluids was demonstrated in Murrone & Guillard (2004), Perigaud & Saurel (2005) and Petitpas *et al.* (2007). It was extended in Perigaud & Saurel (2005) to capillary and viscous effects. Unlike to the Cahn & Hilliard (1958) model, the interface has no capillary length scale. This has important consequences for numerical resolution as well as its ability to deal with large density ratios. Another important difference is thermodynamic closure. Two pure-phase EOS are used instead of a single one, like that of van der Waals. The model remains away from thermal equilibrium and the presence of temperature and chemical potential differences will be used below to derive a relaxation model able to deal with evaporation fronts.

This last model is the starting point of the present analysis. Its derivation in the presence of heat and mass transfer is detailed below. Its thermodynamic closure, based on two equations of state, is detailed. The construction of kinetic terms that make the system relax toward equilibrium is done on the basis of the entropy inequality. With this kinetic closure and special treatment of stiff relaxation, the model is shown to be able to compute evaporation fronts by solving their internal structure. Metastable states are involved, as well as shock, rarefaction and interface dynamics. The dynamic appearance of cavitation pockets is studied in the following limit situations:

(i) simple mechanical pocket growth,

(ii) mechanical pocket growth with heat and mass exchanges.

3. The flow model when there is no mass transfer

The present approach is based on a five-equation model with a single pressure and a single velocity but two temperatures and entropies. Mass transfers will be modelled as relaxation effects. Before doing this, the flow model in the absence of mass transfer is derived. It is obtained in the asymptotic limit of a non equilibrium two-phase, two-pressure and two-velocity hyperbolic multiphase flow model. The following asymptotic reduction follows the lines of Kapila *et al.* (2001).

3.1. *The 'parent' model*

The starting point of the present analysis is the Baer & Nunziato (1986) model with symmetric closure relations (Saurel *et al.* 2003; Chinnayya, Daniel & Saurel 2004):

$$\frac{\partial \alpha_1}{\partial t} + \boldsymbol{u}_I \cdot \nabla \alpha_1 = \mu(p_1 - p_2), \quad \frac{\partial \alpha_1 \rho_1}{\partial t} + \operatorname{div}(\alpha_1 \rho_1 \boldsymbol{u}_1) = 0, \tag{3.1a, b}$$

$$\frac{\partial \alpha_1 \rho_1 \boldsymbol{u}_1}{\partial t} + \operatorname{div}(\alpha_1 \rho_k \boldsymbol{u}_k \otimes \boldsymbol{u}_k) + \nabla(\alpha_1 p_1) = p_I \nabla \alpha_1 + \lambda(\boldsymbol{u}_2 - \boldsymbol{u}_1) \tag{3.1c}$$

$$\frac{\partial \alpha_1 \rho_1 E_1}{\partial t} + \operatorname{div}(\alpha_1(\rho_1 E_1 + p_1)\boldsymbol{u}_1) = p_I \boldsymbol{u}_I \cdot \nabla \alpha_1 + \lambda \boldsymbol{u}_I \cdot (\boldsymbol{u}_2 - \boldsymbol{u}_1) - p_I \mu(p_1 - p_2) + Q_1 \tag{3.1d}$$

$$\frac{\partial \alpha_2 \rho_2}{\partial t} + \operatorname{div}(\alpha_2 \rho_2 \boldsymbol{u}_2) = 0, \tag{3.1e}$$

$$\frac{\partial \alpha_2 \rho_2 \boldsymbol{u}_2}{\partial t} + \operatorname{div}(\alpha_2 \rho_k \boldsymbol{u}_k \otimes \boldsymbol{u}_k) + \nabla(\alpha_2 p_2) = p_I \nabla \alpha_2 - \lambda(\boldsymbol{u}_2 - \boldsymbol{u}_1) \tag{3.1f}$$

$$\frac{\partial \alpha_2 \rho_2 E_2}{\partial t} + \operatorname{div}(\alpha_2(\rho_2 E_2 + p_2)\boldsymbol{u}_2) = p_I \boldsymbol{u}_I \cdot \nabla \alpha_2 - \lambda \boldsymbol{u}_I \cdot (\boldsymbol{u}_2 - \boldsymbol{u}_1) + p_I \mu (p_1 - p_2) - Q_1. \tag{3.1g}$$

We denote respectively by α_k, ρ_k, $\boldsymbol{u}_k$, p_k, E_k and e_k the volume fraction, the density, the velocity vector, the pressure, the total specific energy and the internal specific energy of phase k. The total specific energy is defined as $E_k = e_k + \boldsymbol{u}_k^2/2$. Subscripts 1 and 2 refer to the two phases, and I to the interface.

The heat transfer term Q_1 is simply modelled by $Q_1 = H(T_2 - T_1)$ where $H = hS_I$ involves the convective heat transfer coefficient h and the specific exchange surface S_I. This system guarantees conservation for the mixture and is frame invariant.

The interaction terms that appear on the right-hand side express the effects which drive the system to mechanical equilibrium by the way of relaxation coefficients. Following Saurel *et al.* (2003) where the continuous limit of the discrete two-phase flow equations derived in Abgrall & Saurel (2003) is obtained, symmetric closure relations are available:

$$\mu = \frac{S_I}{Z_1 + Z_2}, \qquad \lambda = Z_1 Z_2 \mu,$$

where Z represents the acoustic impedance ($Z = \rho c$). The average interfacial pressure and velocity are given by

$$\begin{aligned} p_I &= \frac{Z_1 p_2 + Z_2 p_1}{Z_1 + Z_2} + \operatorname{sign}\left(\frac{\partial \alpha_1}{\partial x}\right) \frac{(u_2 - u_1) Z_1 Z_2}{Z_1 + Z_2}, \\ u_I &= \frac{Z_1 u_1 + Z_2 u_2}{Z_1 + Z_2} + \operatorname{sign}\left(\frac{\partial \alpha_1}{\partial x}\right) \frac{p_2 - p_1}{Z_1 + Z_2}. \end{aligned} \tag{3.2}$$

The system (3.1) with this choice of interface variables and relaxation coefficient is consistent with the second law of thermodynamics. Other estimates are also possible; one other choice is given by Baer & Nunziato (1986):

$$p_I = p_1, \qquad u_I = u_2. \tag{3.3}$$

In the present study, where stiff mechanical relaxation is considered, the estimates (3.2) and (3.3) can be used interchangeably. However, in the general case of finite relaxation rate, the estimates (3.2) are able to enforce interface conditions at each volume fraction discontinuity (equality of normal velocities and pressure) automatically (Abgrall & Saurel 2003). This system is unconditionally hyperbolic and admits the characteristic wave speeds: $u_k, u_k + c_k, u_k - c_k$ for each phase k and the interface velocity u_I.

For the present application, this system involves unnecessary effects (two velocities and two pressures) and a reduced model is preferred. It is important to determine the simplest model involving the pertinent physics. The reduction of system (3.1) is done in the following subsection.

3.2. *Reduced model*

The two-phase flow model (3.1) can be written using primitive variables, namely

$$\frac{\partial U}{\partial t} = F(U) + \Phi(U),$$

with

$$U = \begin{pmatrix} \alpha_1 \\ \alpha_1\rho_1 \\ \boldsymbol{u}_1 \\ p_1 \\ \alpha_2\rho_2 \\ \boldsymbol{u}_2 \\ p_2 \end{pmatrix}, F(U) = \begin{pmatrix} -\boldsymbol{u}_1\cdot\nabla\alpha_1 \\ -\operatorname{div}(\alpha_1\rho_1\boldsymbol{u}_1) \\ -\boldsymbol{u}_1\cdot\nabla\boldsymbol{u}_1 - \dfrac{1}{\rho_1}\nabla p_1 + \dfrac{p_I - p_1}{\alpha_1\rho_1}\nabla\alpha_1 \\ -\rho_1 c_1^2 \operatorname{div}(\boldsymbol{u}_1) + \dfrac{\Gamma_1}{\alpha_1}\left[p_I - \rho_1^2\left(\dfrac{\partial e_1}{\partial\rho_1}\right)_{p_1}\right](\boldsymbol{u}_I - \boldsymbol{u}_1)\cdot\nabla\alpha_1 \\ -\operatorname{div}(\alpha_2\rho_2\boldsymbol{u}_2) \\ -\boldsymbol{u}_2\cdot\nabla\boldsymbol{u}_2 - \dfrac{1}{\rho_2}\nabla p_2 + \dfrac{p_I - p_2}{\alpha_2\rho_2}\nabla\alpha_2 \\ -\rho_2 c_2^2 \operatorname{div}(\boldsymbol{u}_2) + \dfrac{\Gamma_2}{\alpha_2}\left[p_I - \rho_2^2\left(\dfrac{\partial e_2}{\partial\rho_2}\right)_{p_2}\right](\boldsymbol{u}_I - \boldsymbol{u}_2)\cdot\nabla\alpha_2 \end{pmatrix}$$

and

$$\Phi(U) = \begin{pmatrix} \mu(p_1 - p_2) \\ 0 \\ \dfrac{\lambda}{\alpha_1\rho_1}(\boldsymbol{u}_2 - \boldsymbol{u}_1) \\ -\mu\dfrac{\Gamma_1}{\alpha_1}\left[p_I - \rho_1^2\left(\dfrac{\partial e_1}{\partial\rho_1}\right)_{p_1}\right](p_1 - p_2) + \lambda\dfrac{\Gamma_1}{\alpha_1}(\boldsymbol{u}_I - \boldsymbol{u}_1)(\boldsymbol{u}_2 - \boldsymbol{u}_1) + \dfrac{\Gamma_1}{\alpha_1}Q_1 \\ 0 \\ -\dfrac{\lambda}{\alpha_2\rho_2}(\boldsymbol{u}_2 - \boldsymbol{u}_1) \\ \mu\dfrac{\Gamma_2}{\alpha_2}\left[p_I - \rho_2^2\left(\dfrac{\partial e_2}{\partial\rho_2}\right)_{p_2}\right](p_1 - p_2) - \lambda\dfrac{\Gamma_2}{\alpha_2}(\boldsymbol{u}_I - \boldsymbol{u}_2)(\boldsymbol{u}_2 - \boldsymbol{u}_1) - \dfrac{\Gamma_2}{\alpha_2}Q_1 \end{pmatrix}$$

Here, c_k represents the speed of sound of phase k:

$$\forall k = 1, 2 \qquad c_k^2 = \frac{\dfrac{p_k}{\rho_k^2} - \left(\dfrac{\partial e_k}{\partial\rho_k}\right)_{p_k}}{\left(\dfrac{\partial e_k}{\partial p_k}\right)_{\rho_k}},$$

and Γ_k represents the Gruneisen coefficient of phase k:

$$\forall k = 1, 2 \qquad \Gamma_k = v_k\left(\frac{\partial p_k}{\partial e_k}\right)_{\rho_k}$$

where $v_k = 1/\rho_k$.

The reduced system is obtained in the limit of stiff mechanical relaxation:

$$\mu = \frac{1}{\epsilon}, \lambda = \frac{1}{\epsilon} \quad \text{where} \quad \epsilon \to 0^+.$$

Note that infinite relaxation parameters are consistent with the expression of pressure and velocity relaxation parameters linked by the relation $\lambda = Z_1 Z_2 \mu$. It is also important to note that heat transfer effects are not considered in the same limit, as we are seeking a temperature non-equilibrium model.

With this notation, the preceding system becomes

$$\frac{\partial U}{\partial t} = F(U) + \frac{1}{\epsilon}\Psi(U) + Q(U) \tag{3.4}$$

with

$$\Psi(U) = \begin{pmatrix} (p_1 - p_2) \\ 0 \\ \dfrac{Z_1 Z_2}{\alpha_1 \rho_1}(\boldsymbol{u}_2 - \boldsymbol{u}_1) \\ -\dfrac{\Gamma_1}{\alpha_1} K_1 (p_1 - p_2) + \dfrac{Z_1 Z_2 \Gamma_1}{\alpha_1}(\boldsymbol{u}_I - \boldsymbol{u}_1)(\boldsymbol{u}_2 - \boldsymbol{u}_1) \\ 0 \\ -\dfrac{Z_1 Z_2}{\alpha_2 \rho_2}(\boldsymbol{u}_2 - \boldsymbol{u}_1) \\ \dfrac{\Gamma_2}{\alpha_2} K_2 (p_1 - p_2) - \dfrac{Z_1 Z_2 \Gamma_2}{\alpha_2}(\boldsymbol{u}_I - \boldsymbol{u}_2)(\boldsymbol{u}_2 - \boldsymbol{u}_1) \end{pmatrix}, \quad Q(U) = \begin{pmatrix} 0 \\ 0 \\ 0 \\ \dfrac{\Gamma_1}{\alpha_1} Q_1 \\ 0 \\ 0 \\ -\dfrac{\Gamma_2}{\alpha_2} Q_1 \end{pmatrix}$$

Here, F and Ψ are regular functions evaluated at a state U which is close to the mechanical equilibrium state U_0. We can set

$$U^\epsilon = U_0 + \epsilon U_1 + O(\epsilon^2)$$

and system (3.4) becomes

$$\frac{\partial U_0}{\partial t} + \epsilon \frac{\partial U_1}{\partial t} = F(U_0) + \epsilon \frac{\partial F(U)}{\partial U}(U_0) U_1 + \frac{1}{\epsilon}\Psi(U_0) + \frac{\partial \Psi(U)}{\partial U}(U_0) U_1 + Q(U_0) + \epsilon \frac{\partial Q(U)}{\partial U}(U_0) U_1 + O(\epsilon^2).$$

Since U_0 is an equilibrium state,

$$\Psi(U_0) = 0 \tag{3.5}$$

and in the system in reduced form becomes

$$\frac{\partial U_0}{\partial t} = F(U_0) + \frac{\partial \Psi(U)}{\partial U}(U_0) U_1 + Q(U_0). \tag{3.6}$$

Condition (3.5) implies that in the asymptotic state, the system has to satisfy

$$\boldsymbol{u}_1^0 = \boldsymbol{u}_2^0 = \boldsymbol{u}^0$$

and

$$p_1^0 = p_2^0 = p^0.$$

These constraints used in (3.6) give the reduced model that takes into account heat transfer effects:

$$\left.\begin{aligned} &\frac{\partial \alpha_1}{\partial t} + \boldsymbol{u}\cdot\nabla\alpha_1 = K(\alpha_1, \rho_1, \rho_2, p)\,\mathrm{div}(\boldsymbol{u}) + \frac{\alpha_1\alpha_2}{\alpha_2\rho_1 c_1^2 + \alpha_1\rho_2 c_2^2}\left(\frac{\Gamma_1}{\alpha_1} + \frac{\Gamma_2}{\alpha_2}\right) Q_1, \\ &\frac{\partial \alpha_1\rho_1}{\partial t} + \mathrm{div}(\alpha_1\rho_1\boldsymbol{u}) = 0, \quad \frac{\partial \alpha_2\rho_2}{\partial t} + \mathrm{div}(\alpha_2\rho_2\boldsymbol{u}) = 0, \\ &\frac{\partial \rho\boldsymbol{u}}{\partial t} + \mathrm{div}(\rho\boldsymbol{u}\otimes\boldsymbol{u}) + \nabla p = 0, \quad \frac{\partial \rho E}{\partial t} + \mathrm{div}(\boldsymbol{u}(\rho E + p)) = 0, \end{aligned}\right\} \tag{3.7}$$

where $K = \alpha_1\alpha_2(\rho_2 c_2^2 - \rho_1 c_1^2)/(\alpha_2\rho_1 c_1^2 + \alpha_1\rho_2 c_2^2)$. The superscript 0 has been omitted for clarity. The mixture variables are defined by: $\rho = \alpha_1\rho_1 + \alpha_2\rho_2$ and $E = Y_1 E_1 + Y_2 E_2$, where $Y_k = \alpha_k\rho_k/\rho$ denotes the mass fraction of phase k.

4. Thermodynamic closure

In order to circumvent the difficulty of models having negative squared speed of sound in the two-phase region, the present model uses two equations of state (EOS). Each fluid possesses its own EOS. In the present paper, we consider stiffened gas (SG) equations of state, but the method can be generalized to more complex convex equations of state. The SG EOS or its generalized form (Mie–Gruneisen (MG) EOS) are usually used for shock dynamics in condensed materials. The parameters used in these EOS are determined by using a reference curve, usually in the (p, v)-plane. In shock physics, the Hugoniot curve is used. A discussion of MG and SG EOS is given in Menikoff & Plohr (1989). It is also possible to use another reference curve to determine EOS parameters. In Le Metayer, Massoni & Saurel (2004) saturation curves are used to determine SG parameters for liquid and vapour phases. These curves are more relevant for phase transition. However, the SG EOS is a linear approximation of the saturation curve in the (p, v)-plane. Thus, it is valid in a limited range of pressure and specific volumes, as reported in Le Metayer *et al.* (2004) and in this section. If necessary, accuracy can be improved by using a nonlinear approximation of the saturation curve, for example with the MG formulation, but this is outside the scope of the present paper.

Our goal in using the SG EOS is to handle the essentials of the physics and thermodynamics under a simple analytical formulation. Moreover this EOS is the simplest prototype that contains the main physical properties of pure fluids: attractive and repulsive molecular effects. Thus, each fluid has its own thermodynamics and in particular its own entropy. In the present modelling of mass transfer, detailed in the next section, relaxation towards equilibrium is achieved by a kinetic process, unlike to van der Waals modelling where mass transfer is a thermodynamic path. This is the reason why the present modelling preserves hyperbolicity during mass transfer.

However, when equilibrium is reached, conventional properties of the phase diagram have to be recovered (latent heat of vaporization, saturation temperature) that depend on pressure or temperature. In other words, the two pure-fluid EOS must be connected by some constraints. These constraints are used for the determination of the various constants involved in these EOS.

For each phase the thermodynamic state is determined by the SG EOS:

$$e(p, v) = \frac{p + \gamma p_\infty}{(\gamma - 1)} v + q, \tag{4.1a}$$

$$v(p, T) = \frac{(\gamma - 1) C_v T}{p + p_\infty}, \tag{4.1b}$$

$$h(T) = \gamma C_v T + q, \tag{4.1c}$$

$$g(p, T) = (\gamma C_v - q')T - C_v T \log \frac{T^\gamma}{(p + p_\infty)^{(\gamma - 1)}} + q, \tag{4.1d}$$

where e, $v = 1/\rho$, p, T, h and g are respectively the internal energy, the specific volume, the pressure, the temperature, the enthalpy and the Gibbs free energy of the considered phase. The constants, characteristic of each fluid, are: γ, p_∞, C_v, q and q'.

A method to determine these parameters in gas–liquid systems is given in Le Metayer *et al.* (2004). The coupling of gas and liquid parameters is examined particularly. This method is summarized below.

4.1. *Method to determine SG EOS parameters*

Parameters of the SG EOS are determined from experimental curves for each fluid. In the case we are interested in (liquid in the presence of its vapour), we need the saturation curves. The experimental data needed are: $p = p_{sat}(T)$, $h_{l,exp}(T)$, $h_{g,exp}(T)$, $v_{l,exp}(T)$, $v_{g,exp}(T)$ and the latent heat of vaporization $L_{v,exp}(T) = h_{g,exp}(T) - h_{l,exp}(T)$.

(*a*) From the expression for enthalpy (4.1*c*), we have

$$\forall k = l, g: \quad \frac{\mathrm{d}h_k}{\mathrm{d}T} = \gamma_k C_{v,k} = C_{p,k}.$$

This permits the average heat capacity coefficients $C_{p,k}$ to be determined by a linear approximation between two reference states 0 and 1 as

$$\forall k = l, g: \quad C_{p,k} = \frac{h_{k,exp}(T_1) - h_{k,exp}(T_0)}{T_1 - T_0}.$$

This also allows the calculation of the reference energies:

$$\forall k = l, g: \quad q_k = h_{k,exp}(T_0) - C_{p,k} T_0.$$

(*b*) Then, by using the experimental curve $p = p_{sat}(T)$, the specific volume is expressed as

$$\forall k = l, g: \quad v_k(T) = \frac{(C_{p,k} - C_{v,k})T}{p_{sat}(T) + p_{\infty,k}}. \tag{4.2}$$

Under logarithmic differentiation, we have

$$\forall k = l, g: \quad \mathrm{d} \log v_k(T)) = \mathrm{d} \log(T) - \mathrm{d} \log (p_{sat}(T) + p_{\infty,k}).$$

The integration of this equation between the two reference states 0 and 1 yields $\forall k = l, g$:

$$\log(v_k(T_1)) - \log(v_k(T_0)) = \log(T_1) - \ln(T_0) - \log(p_{sat}(T_1) + p_{\infty,k}) + \log(p_{sat}(T_0) + p_{\infty,k})$$

This expression allows the calculation of the coefficients $p_{\infty,k}$:

$$\forall k = l, g: \qquad p_{\infty,k} = \frac{v_k(T_0) T_1 p_{sat}(T_0) - v_k(T_1) T_0 p_{sat}(T_1)}{v_k(T_1) T_0 - v_k(T_0) T_1}$$

(*c*) Then (4.2) applied to the reference state 0 provides the approximation of $C_{v,k}$:

$$\forall k = l, g: \qquad C_{v,k} = C_{p,k} - \frac{v_k(T_0)}{T_0}(p_{sat}(T_0) + p_{\infty,k}).$$

(*d*) The approximation for γ_k follows:

$$\forall k = l, g: \quad \gamma_k = \frac{C_{p,k}}{C_{v,k}}.$$

(*e*) At thermodynamic equilibrium, the two Gibbs free energies have to be equal ($g_g = g_l$) with the definition (4.1*d*). This implies

$$\log(p + p_{\infty,v}) = A + \frac{B}{T} + C\log(T) + D\log(p + p_{\infty,l}) \tag{4.3}$$

where A, B, C and D depend on the SG EOS parameters:

$$A = \frac{C_{p,l} - C_{p,g} + q'_g - q'_l}{C_{p,g} - C_{v,g}}, \quad B = \frac{q_l - q_g}{C_{p,g} - C_{v,g}}, \quad C = \frac{C_{p,g} - C_{p,l}}{C_{p,g} - C_{v,g}},$$
$$D = \frac{C_{p,l} - C_{v,l}}{C_{p,g} - C_{v,g}}.$$

Relation (4.3) is nonlinear but permits the computation of the theoretical curve $p = p_{sat}(T)$. Such a computation needs the two entropy constants q'. By convention, we take $q'_l = 0$ J kg^{-1} K^{-1} and choose q'_g in order to obtain the best fit between theoretical and experimental curves.

This algorithm for the determination of the SG EOS parameters is very accurate provided that experimental saturation curves are quasi-linear. This means that the two reference states have to be sufficiently close. Near the critical point, restrictions appear. But far from this point, wide ranges of temperatures and pressures can be covered as shown below.

4.2. *Results for water and dodecane*

As an illustration, results concerning liquid and vapour water and liquid and vapour dodecane are presented.

For water, the chosen temperature range is 298–473 K. The corresponding experimental data (Oldenbourg 1989) are

$$p_{sat}(T_0) = 3166\,\text{Pa}, \quad h_{l,exp}(T_0) = 104.7 \times 10^3\,\text{J}/\text{K}^{-1}\text{g}^{-1},$$
$$h_{g,exp}(T_0) = 2473.4 \times 10^3\,\text{J K}^{-1}\,\text{g}^{-1}, \quad v_{g,exp}(T_0) = 42.4\,\text{m}^3\,\text{K}^{-1}\,\text{g}^{-1},$$
$$p_{sat}(T_1) = 15.5 \times 10^5\,\text{Pa}, \quad h_{l,exp}(T_1) = 851.6 \times 10^3\,\text{J K}^{-1}\,\text{g}^{-1},$$
$$h_{g,exp}(T_1) = 2733.7 \times 10^3\,\text{J K}^{-1}\,\text{g}^{-1}, \quad v_{g,exp}(T_1) = 0.124\,\text{m}^3\,\text{K}^{-1}\,\text{g}^{-1}.$$

The results of the algorithm in § 4.1 are summarized in table 1 and a comparison between experimental and SG approximation curves is shown in figure 5. Obviously, some errors are present, essentially regarding the liquid specific volume where a 25 % maximum error is seen. The reason is that the SG EOS is the simplest prototype involving repulsive and attractive potentials for condensed materials. With this particularly simple formulation it is possible to fit quite well saturation curves and phase diagram. If better accuracy is required, a more sophisticated model can be used (MG EOS for example), at the price of a more cumbersome method to determine the various constants. Our aim is not to construct EOS in this paper but

	p_∞ (Pa)	C_p (J kg^{-1}K^{-1})	C_v (J kg^{-1}K^{-1})	γ	q (J kg^{-1})	q' (J kg^{-1}K^{-1})
liquid	10^9	4267	1816	2.35	-1167×10^3	0
vapour	0	1487	1040	1.43	2030×10^3	-23×10^3

TABLE 1. SG EOS parameters for liquid and vapour water.

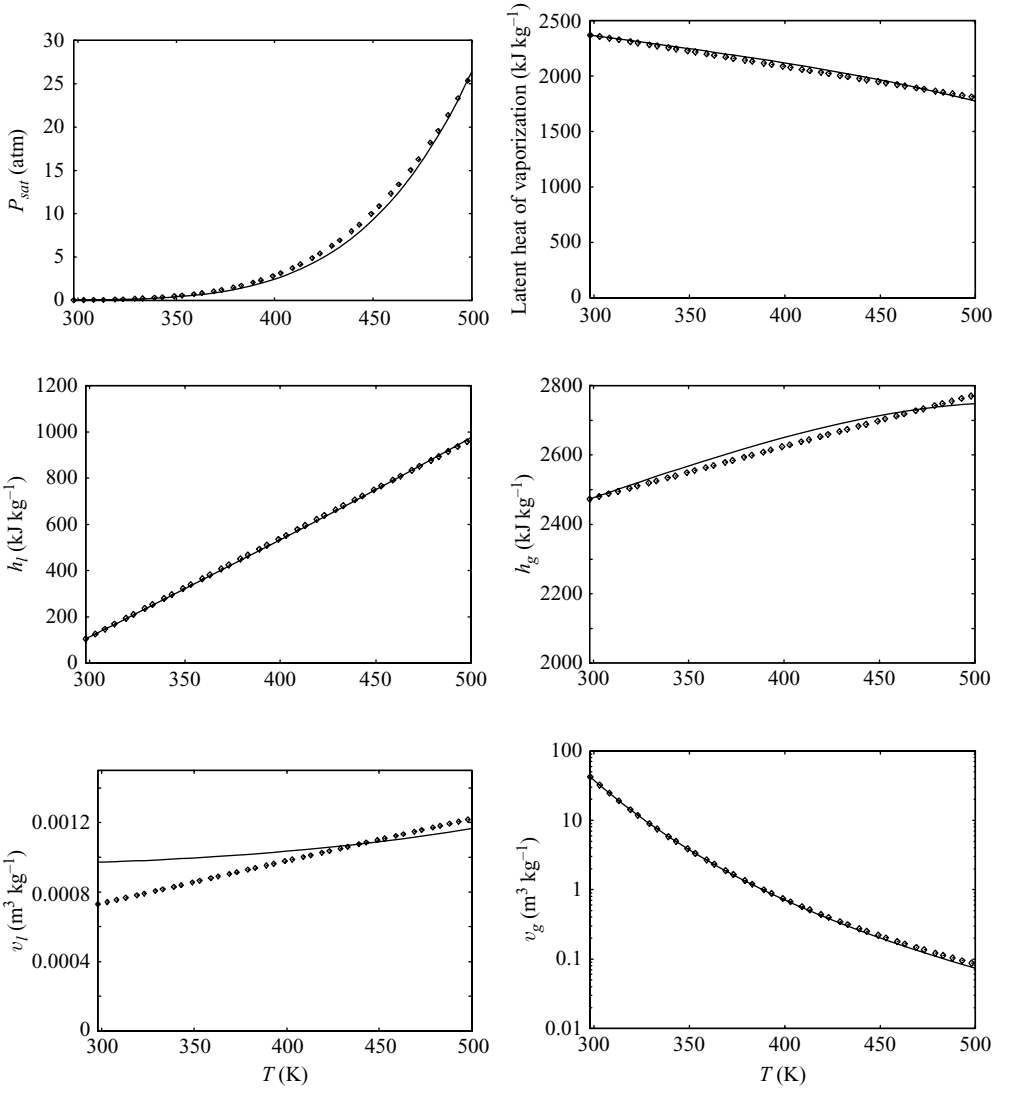

FIGURE 5. Saturation curves for water in the temperature range 298–473 K. Experimental curves are shown with lines and the stiffened gas approximation with symbols.

to propose a general technique. The problem of defining a proper equation of state has been considered in Le Metayer *et al.* (2004) and the method we propose in this paper can be applied to more general EOS without special conceptual difficulty. Once again, our aim is more to show that the new multiphase model, under simplified

	p_∞ (Pa)	C_p (J kg^{-1} K^{-1})	C_v (J kg^{-1} K^{-1})	γ	q (J kg^{-1})	q'(J kg^{-1} K^{-1})
liquid	4×10^8	2534	1077	2.35	-755×10^3	0
vapour	0	2005	1956	1.025	-237×10^3	-24×10^3

TABLE 2. SG EOS parameters for liquid dodecane and its vapour

thermodynamic closure, is able to deal with evaporation waves and metastable states with reasonable accuracy.

The same algorithm is used to determine thermodynamic parameters of dodecane, in the temperature range 298–473 K. A phase diagram and associated data are available in Simoes-Moreira (1994). The corresponding SG EOS parameters are summarized in table 2. The same accuracy as for water when compared with experimental data was seen.

4.3. *Mixture SG EOS*

With the help of the EOS of the phases, the mixture EOS is easily obtained. The mixture specific internal energy definition is

$$\rho e = \alpha_1 \rho_1 e_1 + \alpha_2 \rho_2 e_2.$$

By using SG EOS (4.1*a*), each product $\rho_k e_k$ can be written

$$\rho_k e_k = \frac{p_k + \gamma_k p_{\infty,k}}{\gamma_k - 1} + \rho_k q_k.$$

Under pressure equilibrium, we obtain the closure relation for system (3.7):

$$p(\rho, e, \alpha_1, \alpha_2, Y_1, Y_2) = \frac{\rho(e - Y_1 q_1 - Y_2 q_2) - \left(\dfrac{\alpha_1 \gamma_1 p_{\infty,1}}{\gamma_1 - 1} + \dfrac{\alpha_2 \gamma_2 p_{\infty,2}}{\gamma_2 - 1} \right)}{\dfrac{\alpha_1}{\gamma_1 - 1} + \dfrac{\alpha_2}{\gamma_2 - 1}} \tag{4.4}$$

With this mixture EOS, the flow model (3.7) reproduces propagation of acoustic disturbance at the Wood speed of sound (Wood 1930):

$$\frac{1}{\rho c_w^2} = \frac{\alpha_1}{\rho_1 c_1^2} + \frac{\alpha_2}{\rho_2 c_2^2}. \tag{4.5}$$

This sound speed has a non-monotonic behaviour versus volume fraction, as shown in figure 6. The system (3.7) is strictly hyperbolic with the characteristic waves speeds $u + c_w$, $u - c_w$ and u.

5. Mass transfer modelling

5.1. *Basic ideas*

As mentioned in § 2, it is well known (Menikoff & Plohr 1989) that van der Waals or cubic EOS used in the context of the Euler or Navier–Stokes equations correspond to ill-posed models. The square of the sound speed becomes negative in the spinodal zone. Our model considers phase change as a kinetic transformation and not as a thermodynamic one. The phase diagram in figure 7 illustrates both options. With the kinetic representation, metastable states are present, and the mixture sound speed is always defined. Such an approach poses extra difficulties however:

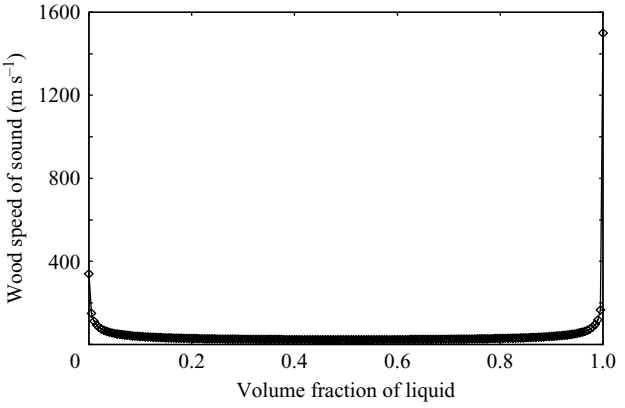

FIGURE 6. Wood's speed of sound versus liquid volume fraction for a liquid–vapour water mixture.

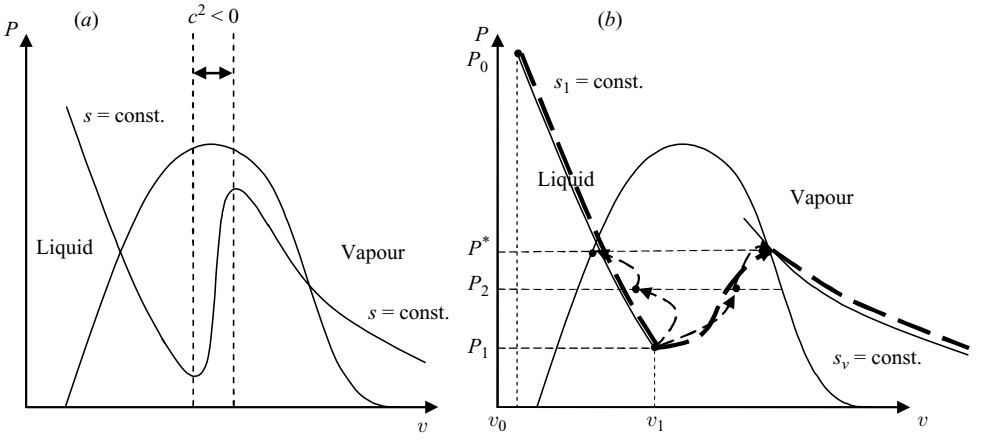

FIGURE 7. Schematic representation of the thermodynamic path using a cubic EOS compared to the kinetic process represented in dashed lines. (*a*) With the cubic EOS, hyperbolicity is lost in the spinodal zone. (*b*) The present model consists of using a kinetic transformation to connect the isentropes of liquid and vapour. As no thermodynamic path is involved, the mixture sound speed is always defined. In the kinetic approach, from a metastable liquid (end of liquid isentrope) non-equilibrium vapour and liquid are produced at constant specific volume for the mixture. Vapour production makes the pressure increase. During kinetic evolution the non-equilibrium points of liquid and vapour move in the direction of saturation curves. At each non-equilibrium state pressure equilibrium is assumed. When thermodynamic equilibrium is reached, liquid and vapour states are located on saturation curves. Then, if the specific volume is increased, the equilibrium concentration evolves and as limit case, the vapour expands along an isentrope starting from the saturation curve. Note that when the various non-equilibrium states are omitted, the global transformation path (the bold dashed line), composed of two thermodynamic paths and a kinetic one, gives a transformation very closed to that of van der Waals. The main difference is that ill-posedness issues have been removed.

(i) determination of the phases EOS – this issue has been examined previously;
(ii) determination of mass transfer terms.

The system (3.7) describes a compressible two-phase flow mixture in mechanical equilibrium but not in thermal equilibrium. The goal is now to introduce mass transfer effects. The addition of mass transfer modifies the mass equation of each

fluid:

$$\frac{\partial \alpha_1 \rho_1}{\partial t} + \operatorname{div}(\alpha_1 \rho_1 \boldsymbol{u}) = \rho \dot{Y}_1,$$

$$\frac{\partial \alpha_2 \rho_2}{\partial t} + \operatorname{div}(\alpha_2 \rho_2 \boldsymbol{u}) = -\rho \dot{Y}_1,$$

where $\rho \dot{Y}_1$ represents the mass flux from fluid 2 to fluid 1. Mass transfer is considered with a finite rate, which means that it has no dependence on the small parameter ϵ. An expression for this mass flux has to be determined.

Mass transfer implies changes in the volume fraction. We assume that the volume fraction equation becomes

$$\frac{\partial \alpha_1}{\partial t} + \boldsymbol{u} \cdot \nabla \alpha_1 = K \operatorname{div}(\boldsymbol{u}) + \frac{\alpha_1 \alpha_2}{\alpha_2 \rho_1 c_1^2 + \alpha_1 \rho_2 c_2^2} \left(\frac{\Gamma_1}{\alpha_1} + \frac{\Gamma_2}{\alpha_2} \right) Q_1 + \frac{\rho \dot{Y}_1}{\rho_I} \tag{5.1}$$

where the interfacial density ρ_I has to be determined. The determination of the expressions for mass transfer $\dot{Y}_1$ and interface density ρ_I is based upon the analysis of the entropy production. To this end, the first step is to determine the entropy equation for each fluid.

5.2. *Determination of the entropy equations of the phases*

The entropy equations are determined as solutions of an algebraic system based on:

(i) energy conservation of the mixture,

(ii) pressure equilibrium between phases.

Let us first examine the constraint given by energy conservation to the entropy equations. By using the energy and momentum equations of system (3.7), a simpler form of the energy equation is obtained:

$$\frac{\mathrm{d}e}{\mathrm{d}t} + p \frac{\mathrm{d}v}{\mathrm{d}t} = 0 \tag{5.2}$$

where the mixture internal energy is defined by $e = Y_1 e_1 + Y_2 e_2$ and the mixture specific volume is given by $v = Y_1 v_1 + Y_2 v_2$. Thus (5.2) becomes

$$Y_1 \left(\frac{\mathrm{d}e_1}{\mathrm{d}t} + p \frac{\mathrm{d}v_1}{\mathrm{d}t} \right) + Y_2 \left(\frac{\mathrm{d}e_2}{\mathrm{d}t} + p \frac{\mathrm{d}v_2}{\mathrm{d}t} \right) + (h_1 - h_2) \dot{Y}_1 = 0.$$

Here $h_k = e_k + p v_k$ is the enthalpy of phase k. By using the Gibbs identity for each phase k, we have

$$\frac{\mathrm{d}e_k}{\mathrm{d}t} + p \frac{\mathrm{d}v_k}{\mathrm{d}t} = T_k \frac{\mathrm{d}s_k}{\mathrm{d}t}.$$

The mixture energy conservation now becomes

$$Y_1 T_1 \frac{\mathrm{d}s_1}{\mathrm{d}t} + Y_2 T_2 \frac{\mathrm{d}s_2}{\mathrm{d}t} + (h_1 - h_2) \dot{Y}_1 = 0. \tag{5.3}$$

This last equation involves the two functions $\mathrm{d}s_1/\mathrm{d}t$ and $\mathrm{d}s_2/\mathrm{d}t$ that we want to determine.

A second equation is provided by the mechanical equilibrium condition:

$$p_1(\rho_1, s_1) = p_2(\rho_2, s_2), \tag{5.4}$$

from which we get

$$\left(\frac{\partial p_1}{\partial \rho_1} \right)_{s_1} \frac{\mathrm{d}\rho_1}{\mathrm{d}t} + \left(\frac{\partial p_1}{\partial s_1} \right)_{\rho_1} \frac{\mathrm{d}s_1}{\mathrm{d}t} = \left(\frac{\partial p_2}{\partial \rho_2} \right)_{s_2} \frac{\mathrm{d}\rho_2}{\mathrm{d}t} + \left(\frac{\partial p_2}{\partial s_2} \right)_{\rho_2} \frac{\mathrm{d}s_2}{\mathrm{d}t}.$$

The definition of the speed of sound and Gruneisen coefficient for each phase enables us to write

$$\text{for } k = 1, 2: \qquad \left(\frac{\partial p_k}{\partial \rho_k}\right)_{s_k} = c_k^2 \qquad \text{and} \qquad \left(\frac{\partial p_k}{\partial s_k}\right)_{\rho_k} = \rho_k \Gamma_k \; T_k.$$

The mechanical equilibrium condition (5.4) becomes

$$c_1^2 \frac{\mathrm{d}\rho_1}{\mathrm{d}t} + \rho_1 \Gamma_1 \; T_1 \frac{\mathrm{d}s_1}{\mathrm{d}t} = c_2^2 \frac{\mathrm{d}\rho_2}{\mathrm{d}t} + \rho_2 \Gamma_2 \; T_2 \frac{\mathrm{d}s_2}{\mathrm{d}t}. \tag{5.5}$$

Equations (5.3) and (5.5) form a system of two equations with the two unknown functions $\mathrm{d}s_1/\mathrm{d}t$ and $\mathrm{d}s_2/\mathrm{d}t$, and then we get

$$\frac{\alpha_1\rho_1\alpha_2\rho_2}{\rho} T_1 \left(\frac{\Gamma_1}{\alpha_1} + \frac{\Gamma_2}{\alpha_2}\right) \frac{\mathrm{d}s_1}{\mathrm{d}t} = Y_2 \left(c_2^2 \frac{\mathrm{d}\rho_2}{\mathrm{d}t} - c_1^2 \frac{\mathrm{d}\rho_1}{\mathrm{d}t}\right) - \rho_2 \Gamma_2 (h_1 - h_2) \dot{Y}_1, \tag{5.6a}$$

$$\frac{\alpha_1\rho_1\alpha_2\rho_2}{\rho} T_2 \left(\frac{\Gamma_1}{\alpha_1} + \frac{\Gamma_2}{\alpha_2}\right) \frac{\mathrm{d}s_2}{\mathrm{d}t} = -Y_1 \left(c_2^2 \frac{\mathrm{d}\rho_2}{\mathrm{d}t} - c_1^2 \frac{\mathrm{d}\rho_1}{\mathrm{d}t}\right) - \rho_1 \Gamma_1 (h_1 - h_2) \dot{Y}_1, \tag{5.6b}$$

The next step is to replace the variation $\mathrm{d}\rho_1/\mathrm{d}t$ and $\mathrm{d}\rho_2/\mathrm{d}t$ by variations of the volume fraction and velocity divergence with the help of the mass equations. The system (5.6) now becomes

$$\begin{aligned} \frac{\alpha_1\rho_1\alpha_2\rho_2}{\rho} T_1 \left(\frac{\Gamma_1}{\alpha_1} + \frac{\Gamma_2}{\alpha_2}\right) \frac{\mathrm{d}s_1}{\mathrm{d}t} &= Y_2 \left[\left(\frac{\rho_1 c_1^2}{\alpha_1} + \frac{\rho_2 c_2^2}{\alpha_2}\right) \frac{\mathrm{d}\alpha_1}{\mathrm{d}t} - \left(\rho_2 c_2^2 - \rho_1 c_1^2\right) \operatorname{div}(\boldsymbol{u}) \right] \\ &\quad - \rho Y_2 \left(\frac{c_1^2}{\alpha_1} + \frac{c_2^2}{\alpha_2}\right) \dot{Y}_1 - \rho_2 \Gamma_2 (h_1 - h_2) \dot{Y}_1, \end{aligned} \tag{5.7a}$$

$$\begin{aligned} \frac{\alpha_1\rho_1\alpha_2\rho_2}{\rho} T_2 \left(\frac{\Gamma_1}{\alpha_1} + \frac{\Gamma_2}{\alpha_2}\right) \frac{\mathrm{d}s_2}{\mathrm{d}t} &= -Y_1 \left[\left(\frac{\rho_1 c_1^2}{\alpha_1} + \frac{\rho_2 c_2^2}{\alpha_2}\right) \frac{\mathrm{d}\alpha_1}{\mathrm{d}t} - \left(\rho_2 c_2^2 - \rho_1 c_1^2\right) \operatorname{div}(\boldsymbol{u}) \right] \\ &\quad + \rho Y_1 \left(\frac{c_1^2}{\alpha_1} + \frac{c_2^2}{\alpha_2}\right) \dot{Y}_1 - \rho_1 \Gamma_1 (h_1 - h_2) \dot{Y}_1. \end{aligned} \tag{5.7b}$$

Then by using the volume fraction equation (5.1), the entropy equations become functions only of heat exchange, mass transfer and interfacial density ρ_I:

$$\begin{aligned} Y_1 \frac{\mathrm{d}s_1}{\mathrm{d}t} &= \frac{H(T_2 - T_1)}{\rho T_1} - \frac{\dot{Y}_1 (h_1 - h_2)}{\dfrac{\Gamma_1 T_1}{\alpha_1}\left(\dfrac{\alpha_1}{\Gamma_1} + \dfrac{\alpha_2}{\Gamma_2}\right)} \\ &\quad + \frac{\dot{Y}_1}{T_1 \left(\dfrac{\Gamma_1}{\alpha_1} + \dfrac{\Gamma_2}{\alpha_2}\right)} \left(\frac{\dfrac{\rho_1 c_1^2}{\alpha_1} + \dfrac{\rho_2 c_2^2}{\alpha_2}}{\rho_I} - \left(\frac{c_1^2}{\alpha_1} + \frac{c_2^2}{\alpha_2}\right) \right) \end{aligned} \tag{5.8a}$$

$$\begin{aligned} Y_2 \frac{\mathrm{d}s_2}{\mathrm{d}t} &= -\frac{H(T_2 - T_1)}{\rho T_2} - \frac{\dot{Y}_1 (h_1 - h_2)}{\dfrac{\Gamma_2 T_2}{\alpha_2}\left(\dfrac{\alpha_1}{\Gamma_1} + \dfrac{\alpha_2}{\Gamma_2}\right)} \\ &\quad + \frac{\dot{Y}_1}{T_2 \left(\dfrac{\Gamma_1}{\alpha_1} + \dfrac{\Gamma_2}{\alpha_2}\right)} \left(-\frac{\dfrac{\rho_1 c_1^2}{\alpha_1} + \dfrac{\rho_2 c_2^2}{\alpha_2}}{\rho_I} + \left(\frac{c_1^2}{\alpha_1} + \frac{c_2^2}{\alpha_2}\right) \right) \end{aligned} \tag{5.8b}$$

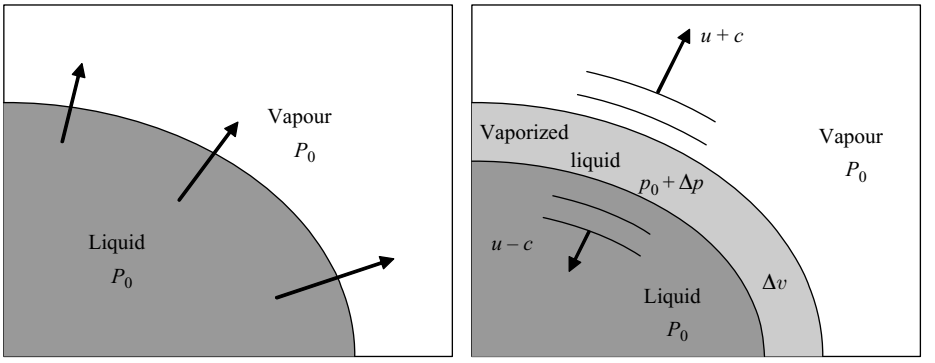

FIGURE 8. Schematic representation of liquid evaporation. An elementary volume Δv of liquid is transformed to vapour with a pressure perturbation. Acoustic waves propagates through liquid and vapour, reflect at volume boundaries and restore pressure equilibrium. The overall process is isentropic as these waves are of small amplitude. These waves are necessarily weak as evaporation is a continuous phenomenon. Elementary volume and pressure perturbations tend to zero.

5.3. *Examination of the entropy production of the phases*

The entropy equation for each phase (5.8) is composed of three terms. Each of them expresses a physical phenomenon responsible for entropy production:

the first one is related to heat exchange,

the second one is associated with mass transfer,

the last term is associated with pressure relaxation process associated with mass transfer. Consider a pressure perturbation appearing during mass transfer, see figure 8. The system returns to mechanical equilibrium with the help of acoustic waves emitted during evaporation. This is similar to acoustic waves emitted by flames. These waves of small amplitude are isentropic.

We thus consider that the pressure relaxation process present during mass transfer is isentropic. This corresponds to the third term on the right-hand side of (5.8) which vanishes. This allows determination of the interface density:

$$\rho_I = \frac{\dfrac{\rho_1 c_1^2}{\alpha_1} + \dfrac{\rho_2 c_2^2}{\alpha_2}}{\dfrac{c_1^2}{\alpha_1} + \dfrac{c_2^2}{\alpha_2}}. \tag{5.9}$$

5.4. *Mixture entropy inequality*

The second principle of thermodynamics applied to the mixture is:

$$\frac{\partial \rho s}{\partial t} + \operatorname{div}(\rho s \boldsymbol{u}) \geqslant 0$$

where the mixture entropy is defined as $s = Y_1 s_1 + Y_2 s_2$.

Using mass equations and expressions (5.8) for the entropies in this inequality leads to

$$\frac{H(T_2 - T_1)^2}{\rho} + (\overline{g}_2 - \overline{g}_1) T_I \dot{Y}_1 \geqslant 0 \tag{5.10}$$

where an 'interface temperature' appears:

$$T_I = \left(\frac{\Gamma_1 T_1}{\alpha_1} + \frac{\Gamma_2 T_2}{\alpha_2}\right) \Big/ \left(\frac{\Gamma_1}{\alpha_1} + \frac{\Gamma_2}{\alpha_2}\right)$$

The extended Gibbs free energies appear:

$$\text{for } k = 1, 2: \qquad \overline{g}_k = h_k - \overline{T} s_k,$$

with h_k the enthalpy of phase k and $\overline{T} = T_1 T_2 / T_I$.

It appears clearly that the first term of (5.10) related to heat exchange is necessarily greater than or equal to zero. The second term will be greater than or equal to zero if we assume that

$$\dot{Y}_1 = \nu(\overline{g}_2 - \overline{g}_1)$$

where ν is a positive relaxation parameter that controls the rate at which the mixture relaxes to thermodynamic equilibrium. This corresponds to the form of mass transfer terms we were seeking. Note that this modelling of relaxation terms guarantees equilibrium conditions of equal temperatures and equal Gibbs free energies.

5.5. *The model*

We now have a symmetric hyperbolic non-equilibrium compressible two-phase flow model with heat and mass exchanges:

$$\frac{\partial \alpha_1}{\partial t} + \boldsymbol{u} \cdot \nabla \alpha_1 = K \operatorname{div}(\boldsymbol{u}) + \frac{\alpha_1 \alpha_2}{\alpha_2 \rho_1 c_1^2 + \alpha_1 \rho_2 c_2^2} \left(\frac{\Gamma_1}{\alpha_1} + \frac{\Gamma_2}{\alpha_2}\right) Q_1 + \frac{\dfrac{\rho_1 c_1^2}{\alpha_1} + \dfrac{\rho_2 c_2^2}{\alpha_2}}{\dfrac{c_1^2}{\alpha_1} + \dfrac{c_2^2}{\alpha_1}} \rho \dot{Y}_1, \tag{5.11a}$$

$$\frac{\partial \alpha_1 \rho_1}{\partial t} + \operatorname{div}(\alpha_1 \rho_1 \boldsymbol{u}) = \rho \dot{Y}_1, \tag{5.11b}$$

$$\frac{\partial \alpha_2 \rho_2}{\partial t} + \operatorname{div}(\alpha_2 \rho_2 \boldsymbol{u}) = -\rho \dot{Y}_1, \tag{5.11c}$$

$$\frac{\partial \rho \boldsymbol{u}}{\partial t} + \operatorname{div}(\rho \boldsymbol{u} \otimes \boldsymbol{u}) + \nabla p = 0, \tag{5.11d}$$

$$\frac{\partial \rho E}{\partial t} + \operatorname{div}(\boldsymbol{u}(\rho E + p)) = 0, \tag{5.11e}$$

where

$$K = \frac{\alpha_1 \alpha_2 \left(\rho_2 c_2^2 - \rho_1 c_1^2\right)}{\alpha_2 \rho_1 c_1^2 + \alpha_1 \rho_2 c_2^2},$$

$$\dot{Y}_1 = \nu(\overline{g}_2 - \overline{g}_1),$$

$$Q_1 = H(T_2 - T_1).$$

The mixture pressure is given by (4.4):

$$p(\rho, e, \alpha_1, \alpha_2, Y_1, Y_2) = \frac{\rho(e - Y_1 q_1 - Y_2 q_2) - \left(\dfrac{\alpha_1 \gamma_1 p_{\infty,1}}{\gamma_1 - 1} + \dfrac{\alpha_2 \gamma_2 p_{\infty,2}}{\gamma_2 - 1}\right)}{\dfrac{\alpha_1}{\gamma_1 - 1} + \dfrac{\alpha_2}{\gamma_2 - 1}}.$$

The determination of the temperature relaxation parameter H for a two-phase mixture with arbitrary interfacial area is a difficult issue, as is that of the phase transition

kinetics parameter ν that depends not only on interfacial area but also on local chemical relaxation. To circumvent these difficulties, we use a solution procedure based on infinite relaxation parameters, but at selected spatial locations only. More precisely, in order to retain metastable states, the relaxation parameters H and ν will be set to zero for locations far from the interfaces. At the interfaces, they will be taken infinite in order to fulfil equilibrium interface conditions with mass transfer. When dealing with interfaces of simple contact, they will be set to zero everywhere. This procedure is summarized by

$$H, \nu = \begin{cases} +\infty & \text{if } \epsilon \leqslant \alpha_1 \leqslant 1-\epsilon \\ 0 & \text{otherwise} \end{cases}$$

5.6. *Limit interface model*

It is interesting to note that this relaxation method corresponds to the local resolution (in fact at the interface only) of the following limit system, corresponding to the mixture Euler equations:

$$\left.\begin{aligned} &\frac{\partial \rho}{\partial t} + \operatorname{div}(\rho \boldsymbol{u}) = 0, \\ &\frac{\partial \rho \boldsymbol{u}}{\partial t} + \operatorname{div}(\rho \boldsymbol{u} \otimes \boldsymbol{u} + p) = 0, \\ &\frac{\partial \rho E}{\partial t} + \operatorname{div}[(\rho E + p)\boldsymbol{u}] = 0, \end{aligned}\right\} \tag{5.12}$$

where the mixture density is $\rho = \alpha_1\rho_1 + \alpha_2\rho_2$ and the mixture internal energy is $\rho e = \alpha_1\rho_1 e_1 + \alpha_2\rho_2 e_2$. The total mixture energy is still defined by $E = e + u^2/2$.

This system is closed by three thermodynamic equilibrium conditions:

$$p_1 = p_2 = p, \tag{5.13}$$

$$T_1 = T_2 = T, \tag{5.14}$$

$$g_1 = g_2. \tag{5.15}$$

With the help of the SG EOS (4.1) with conditions (5.13) and (5.14), each phase variable can be expressed as a function of pressure and temperature. The definitions of mixture density and internal energy are now

$$\left.\begin{aligned} &\rho = \alpha_2[\rho_2(p,T) - \rho_1(p,T)] + \rho_1(p,T), \\ &e = \frac{1}{\rho}[\alpha_2[\rho_2(p,T)e_2(p,T) - \rho_1(p,T)e_1(p,T)] + \rho_1(p,T)e_1(p,T)]. \end{aligned}\right\} \tag{5.16}$$

The condition (5.15) now reduces to the mixture EOS (4.3) and system (5.16) becomes

$$\alpha_2(T) = \frac{\rho - \rho_1(T)}{\rho_2(T) - \rho_1(T)}, \tag{5.17}$$

$$e(T) = \frac{1}{\rho}[\alpha_2(T)[\rho_2(T)e_2(T) - \rho_1(T)e_1(T)] + \rho_1(T)e_1(T)]. \tag{5.18}$$

Equation (5.18) can be solved numerically. It allows the determination of α_2 with (5.17) and p with (4.3). Thus, the system is closed.

The system (5.12) can also be written under primitive variable form:

$$\frac{\mathrm{d}\rho}{\mathrm{d}t} + \rho\frac{\partial u}{\partial x} = 0, \quad \frac{\mathrm{d}u}{\mathrm{d}t} + \frac{1}{\rho}\frac{\partial p}{\partial x} = 0, \quad \frac{\mathrm{d}p}{\mathrm{d}t} + \rho c^2\frac{\partial u}{\partial x} = 0. \tag{5.19}$$

By using the sound speed definition $c^2 = (\partial p/\partial \rho)_s$ the following expression is obtained:

$$\frac{1}{\rho c_{eq}^2} = \frac{\alpha_1}{\rho_1 c_1^2} + \frac{\alpha_2}{\rho_2 c_2^2} + T\left[\frac{\alpha_1 \rho_1}{C_{p,v}}\left(\frac{\mathrm{d}s_1}{\mathrm{d}p}\right)^2 + \frac{\alpha_2 \rho_2}{C_{p,l}}\left(\frac{\mathrm{d}s_2}{\mathrm{d}p}\right)^2\right] \tag{5.20}$$

corresponding to the thermodynamic equilibrium mixture speed of sound. Details are given in Appendix A. The Wood formula (4.5) is recovered with the first two terms of (5.20). This limit model is again hyperbolic with the characteristic waves speeds: $u + c_{eq}$, $u - c_{eq}$ and u.

However, with the algorithm detailed in the following, there is no need to solve (5.12) explicitly. The coupling with chemically inert zones far from evaporation fronts and a diffuse interface zone governed by (5.12) will be done by the numerical procedure described in the next section. It relies on system (5.11).

6. Numerical method

The numerical method to solve the compressible two-phase flow system (5.11) with heat and mass transfer proceeds in two steps. At each time step, the hyperbolic system in the absence of heat and mass transfer is solved. This provides the non-equilibrium hydrodynamic field. Stiff thermal and chemical relaxations are then solved at the interfaces only. The interfaces are detected from knowledge of volume fraction fields.

The basic ingredients of the hyperbolic solver are summarized below following Petitpas *et al.* (2007). This solver is not conventional as the hyperbolic system is not conservative. Conventional Godunov-type schemes or other existing methods are not suitable for its resolution. Then we present a new stiff differential solver specifically derived for the present model. It is used for integration of stiff heat and mass transfer terms.

6.1. *Hyperbolic solver*

The hyperbolic system (5.11) without heat and mass transfer is

$$\left.\begin{aligned}
&\frac{\partial \alpha_1}{\partial t} + \boldsymbol{u}\cdot\nabla\alpha_1 = K(\alpha_1, \rho_1, \rho_2, p)\ \mathrm{div}\,(\boldsymbol{u}),\\
&\frac{\partial \alpha_1\rho_1}{\partial t} + \mathrm{div}\,(\alpha_1\rho_1\boldsymbol{u}) = 0,\\
&\frac{\partial \alpha_2\rho_2}{\partial t} + \mathrm{div}\,(\alpha_2\rho_2\boldsymbol{u}) = 0,\\
&\frac{\partial \rho\boldsymbol{u}}{\partial t} + \mathrm{div}\,(\rho\boldsymbol{u}\otimes\boldsymbol{u}) + \nabla p = 0,\\
&\frac{\partial \rho E}{\partial t} + \mathrm{div}\,[\boldsymbol{u}(\rho E + p)] = 0.
\end{aligned}\right\} \tag{6.1}$$

The volume fraction equation of system (6.1) is not written in conservative form. This raises two important difficulties regarding numerical resolution:

(i) Conventional shock relations are not available. In their absence, the Riemann problem cannot be solved. The Riemann problem is the cornerstone of modern numerical methods to solve hyperbolic systems.

(ii) The average of the volume fraction variable within a computational cell has no physical meaning. Cell averages have meaning only for conservative variables.

Non-conventional shock relations for system (6.1) are proposed in Saurel *et al.* (2007*b*). These relations:

Guarantee conservation of the mixture.

Tend to the single-phase shock relations when one of the phases disappears. They thus guarantee correct behaviour in the single-phase limit. This feature is important for interface problems.

Preserve volume fraction positivity. This is also an important feature for numerical resolution in the presence of material interfaces.

Are symmetric with respect to the phases. This allows a possible extension of the model to an arbitrary number of components.

Are in perfect agreement with experimental shock measurements. It has been validated for more than 100 experimental tests involving a wide range of shock strength, very different acoustic impedance ratios between phases, different initial volume fractions of the phases, different EOS of pure components. See again Saurel *et al.* (2007*b*).

Last, the mixture Hugoniot curve is tangent to the mixture isentrope. This means that multiphase weak shock waves behave like simple compression waves. This feature is also important for the Riemann problem resolution.

These relations are summarized as follows:

$$\left.\begin{aligned} &\text{for } k=1,2; \quad Y_k = Y_k^0, \\ &\rho(u-\sigma) = \rho_0(u_0-\sigma) = m, \\ &p - p_0 + m^2(v - v_0) = 0, \\ &\text{for } k=1,2: \quad e_k - e_k^0 + \frac{p+p_0}{2}\left(v_k - v_k^0\right) = 0. \end{aligned}\right\} \tag{6.2}$$

Thanks to these relations and Riemann invariants, exact or approximate Riemann solvers can be derived (Petitpas *et al.* 2007). Once the Riemann problem is solved, the second difficulty is to average or project the Riemann problem solution onto the computational cell. Because of the volume fraction variable, we cannot use conventional projection methods. Thus a specific relaxation-projection method has been derived in Saurel *et al.* (2007*a*) and Petitpas *et al.* (2007). All details are available in these references.

6.2. *Stiff thermo-chemical solver*

The cell now contains a multiphase mixture in mechanical equilibrium but not in thermal and chemical equilibrium. Indeed, each phase in the cell has its own temperature and Gibbs free energy. In order to fulfil interface conditions in the presence of heat and mass transfer (equal temperatures and chemical potentials) a relaxation method is used. The interface is located by the following procedure:

(i) A cell is considered filled by a pure fluid when its volume and mass fractions are close to 1 (say for example $1-\epsilon_1$ where typically $\epsilon_1 = 10^{-8}$) . The interface corresponds to mixture cells when volumes and mass fractions range between ϵ_2 and $1-\epsilon_2$ (typically, $\epsilon_2 = 10^{-6}$). This second small parameter has to be chosen in order that evaporation occurs only in the interfacial zone and not during expansion waves that produce metastable states; expansion waves induce gas volume fraction increase. If ϵ_2 is taken too close to ϵ_1 evaporation may occur too early and not only in the interfacial zone.

(ii) Mass transfer is allowed if one of the fluids in the mixture cell is metastable ($T_k > T_{sat}(P)$)).

The hydrodynamic evolution having now been obtained by the numerical approximation of system (6.1) the goal is to solve the following system of ordinary differential equations at the interface only:

$$\left.\begin{aligned} &\frac{\partial \alpha_1}{\partial t} = \frac{\alpha_1\alpha_2}{\alpha_2\rho_1c_1^2+\alpha_1\rho_2c_2^2}\left(\frac{\Gamma_1}{\alpha_1}+\frac{\Gamma_2}{\alpha_2}\right)Q_1 + \frac{\dfrac{\rho_1c_1^2}{\alpha_1}+\dfrac{\rho_2c_2^2}{\alpha_2}}{\dfrac{c_1^2}{\alpha_1}+\dfrac{c_2^2}{\alpha_2}}\rho\dot{Y}_1 = S_{\alpha_1},\\ &\frac{\partial \alpha_1\rho_1}{\partial t} = \rho\dot{Y}_1 = S_{Y_1}, \quad \frac{\partial \alpha_2\rho_2}{\partial t} = -\rho\dot{Y}_1,\\ &\frac{\partial \rho \boldsymbol{u}}{\partial t} = 0, \quad \frac{\partial \rho E}{\partial t} = 0. \end{aligned}\right\} \tag{6.3}$$

The integration of this system necessitates closure relations for Q_1 and $\dot{Y}_1$, in particular regarding relaxation parameters H and ν. In order that the model be free of parameters we assume that thermodynamic local equilibrium is reached at the interface at any time. This means that H and ν tend to infinity locally. This assumption is standard at equilibrium interfaces when mass transfer occurs. It does not mean that the entire flow evolves at thermodynamic equilibrium. The states remain not in equilibrium far from interfaces.

In the context of numerical integration, taking infinite relaxation parameters means that the equilibrium has to be reached at the end of each time step. The time step is imposed by CFL restriction of the hydrodynamic system. Using this time step, we determine Q_1 and $\dot{Y}_1$ in order that thermodynamic equilibrium be reached at the end of each time step. To determine these source terms, the equations for the temperatures and Gibbs free energies differences are necessary

$$\frac{\partial \Delta T}{\partial t} = AQ_1 + B\dot{Y}_1, \quad \frac{\partial \Delta g}{\partial t} = A'Q_1 + B'\dot{Y}_1, \tag{6.4}$$

where A, B, A', B' are functions of all flow variables. Their expressions are detailed in Appendix B.

The simplest numerical approximation of these equations is used. Let n and $n+1$ denote two successive time steps. The variables at time t^n are taken equal to those resulting from the numerical integration of system (6.1). The variables at time t^{n+1} denote the end of the integration process, including both hydrodynamic effects and source terms (6.3). The simplest numerical approximation of this ODE system is

$$\left.\begin{aligned} &\frac{(\Delta T)^{n+1}-(\Delta T)^n}{\Delta t} = A^nQ_1^n + B^n\dot{Y}_1^n,\\ &\frac{(\Delta g)^{n+1}-(\Delta g)^n}{\Delta t} = A'^nQ_1^n + B'^n\dot{Y}_1^n. \end{aligned}\right\} \tag{6.5}$$

By imposing that thermodynamic equilibrium is reached at the end of the time step we have $(\Delta T)^{n+1}=0$ and $(\Delta g)^{n+1}=0$. The corresponding heat and mass transfer terms are given by

$$\left.\begin{aligned} Q_1 &= -\frac{B'}{AB'-A'B}\frac{(\Delta T)^n}{\Delta t} + \frac{B}{AB'-A'B}\frac{(\Delta g)^n}{\Delta t},\\ \dot{Y}_1 &= \frac{A'}{AB'-A'B}\frac{(\Delta T)^n}{\Delta t} - \frac{A}{AB'-A'B}\frac{(\Delta g)^n}{\Delta t}. \end{aligned}\right\} \tag{6.6}$$

These approximations of heat and mass transfer terms allow the calculation of source terms S_{α_1} and S_{Y_1} of system (6.3). Nevertheless, there is no guarantee that positivity of the solution be preserved, in particular regarding mass and volume fractions.

A limitation must be placed on these source terms. Let us express the maximum admissible source term for the volume fraction evolution in order to preserve positivity of this variable:

$$S_{max,\alpha_1} = \begin{cases} \dfrac{1-\alpha_1}{\Delta t} & \text{if } S_{\alpha_1} > 0 \\ \dfrac{-\alpha_1}{\Delta t} & \text{otherwise.} \end{cases} \tag{6.7}$$

The same maximum source term is computed for mass fraction positivity. Thus, if $|S_{max,\alpha_1}| > |S_{\alpha_1}|$ and $|S_{max,Y_1}| > |S_{Y_1}|$, the numerical integration can be done with the hydrodynamics time step. Otherwise, equations are stiff and the integration time step has to be reduced. The ratio $R_{\alpha_1} = S_{max,\alpha_1}/S_{\alpha_1}$ is computed and the system (6.3) is integrated over a fraction of the time step, typically: $\Delta t_{chem} = R_{\alpha_1}\Delta t/2$. Successive point integrations are done in order that the complete hydrodynamic step be covered.

With this algorithm, thermodynamic equilibrium is reached very fast and positivity of the solution is preserved. Using this relaxation method corresponds to the local resolution (actually at the interface only) of the limit system, corresponding to the mixture Euler equations (5.12).

7. Numerical results

The aim of this section is to highlight the capabilities of the model in the numerical resolution of interface problems with or without mass transfer. A set of one-dimensional tests are first considered for validation issues. Then two-dimensional tests are addressed for the dynamic creation of super-cavitating flow pockets.

7.1. *Two-phase shock tube without mass transfer*

In this example, the left part of a shock tube is filled with liquid dodecane at high pressure $p_l = 10^8$ Pa with density $\rho_l = 500\,\mathrm{kg\,m^{-3}}$. The right chamber is set at atmospheric pressure and filled with vapour dodecane at density $\rho_v = 2\,\mathrm{kg\,m^{-3}}$. The initial discontinuity is located at $x = 0.75$ m in a 1 m long tube. For numerical reasons, each chamber of the tube contains a weak volume fraction of the other fluid (typically 10^{-8}).

In the first example, the liquid-gas interface is solved as a contact discontinuity: heat and mass transfer are removed. The results are shown at time $t = 473\,\mu$s in figure 9 and consist of three conventional waves. From left to right, a left-facing rarefaction wave propagates through the liquid, the contact discontinuity is moving from left to right and a right-facing shock propagates through dodecane vapour. The numerical solution is compared to the exact one and shows a perfect agreement.

7.2. *Two-phase shock tube with mass transfer*

We now rerun the same test case and consider heat and mass transfer at the interface. The rarefaction wave propagation transforms the stable high-pressure liquid dodecane into a superheated liquid and evaporation has to be considered (figure 10). An additional left-facing wave (evaporation front) appears between the rarefaction wave and the contact discontinuity. It propagates through the superheated liquid and produces a liquid-vapour mixture at thermodynamic equilibrium and high velocity.

Infinite relaxation parameters are used at the interface only. The limit model corresponds to the mixture Euler equations (5.12), for which acoustic disturbances propagate at c_{eq} (5.20). Far from the interface, the Kapila *et al.* (2001) model is solved in the absence of relaxation terms. This model tends to the considered pure fluid Euler equations, for which acoustic disturbances propagate at c_k (the speed of sound

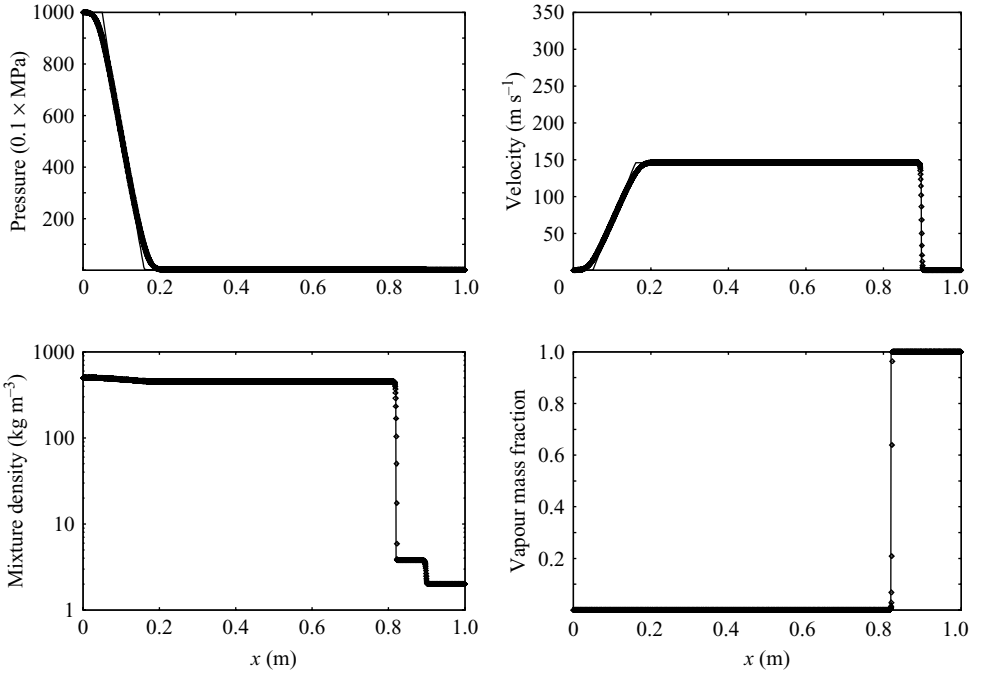

FIGURE 9. Dodecane liquid–vapour shock tube without mass transfer. The numerical solution (symbols) is compared to the exact one (lines). An excellent agreement is observed. The velocity graph scale has been chosen in order that a direct comparison with the results of figure 10 be easy.

of phase k). As c_{eq} is always lower than (or equal to) c_k, acoustic perturbations in pure phases propagate faster than evaporation fronts (whose velocity cannot exceed c_{eq}). Thus, acoustic precursors are present and correspond to expansion or compression waves in pure fluid. They produce metastable states.

We can see the four waves (the left-facing expansion wave, the evaporation front, the contact discontinuity and the right-facing shock as was mentioned in the introduction section and in figure 3) on the mixture density graph of figure 10. The evaporation front makes the vapour mass fraction increase, but total evaporation is not reached. The second jump in mass fraction is related to the contact discontinuity.

The corresponding phase-space trajectory is reported in figure 11 together with the mixture density graph where all fluid states are visible. Stable high-pressure liquid dodecane represented by point 1 is expanded until point 2 with an isentropic path. Point 2 corresponds to metastable liquid dodecane close to the liquid saturation boundary. This point lies inside the saturation dome and is close to the saturation boundary because thermal and chemical relaxation occurs infinitely fast as soon as metastability appears (in the present modelling). The thermal and chemical relaxation transforms the metastable liquid into a liquid–vapour mixture under thermodynamic equilibrium (points 3_l and 3_v). The mixture is now located at point 3 between points 3_l and 3_v, at a specific volume greater than those of point 2. Pressure decreases between points 2 and 3 while specific volume increases as these points belong to the evaporation front, that corresponds here to an expansion wave of the equilibrium system (see figure 13 and related discussion). On the other part of the shock tube, initial vapour (point 5) is shocked and follows a Hugoniot curve until point 4. Points

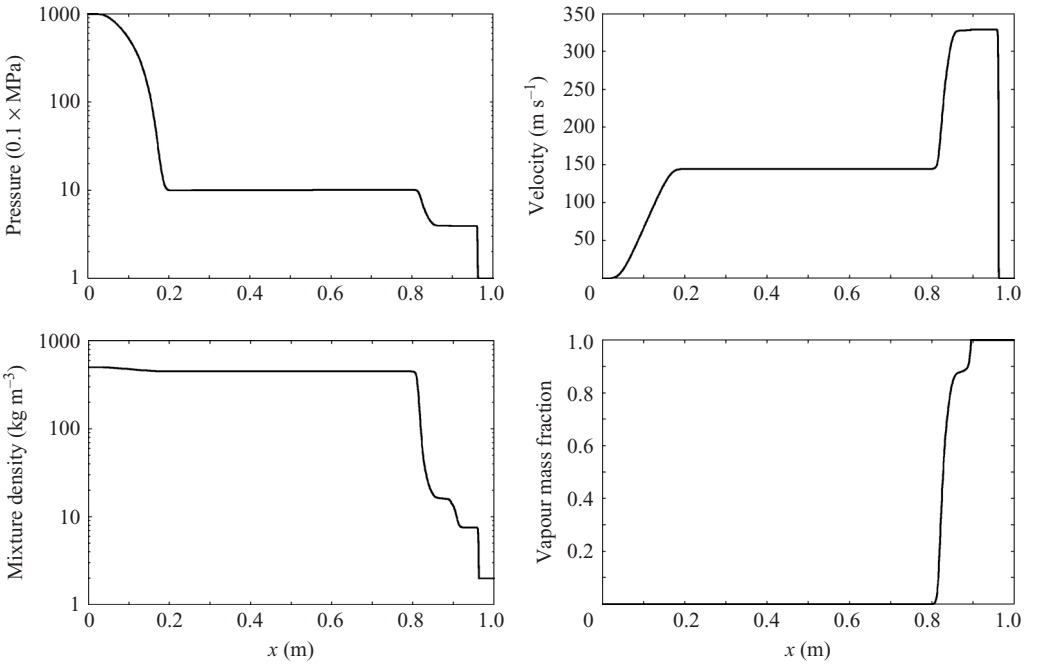

FIGURE 10. Dodecane liquid–vapour shock tube with mass transfer. The thermo-chemical solver is used at the interface. An extra wave appears leading to evaporation of superheated liquid. The second jump in mass fraction is the contact discontinuity between the liquid-vapour mixture produced by evaporation and shocked vapour initially present in the right-hand chamber. The velocity graph can be compared with those of figure 9, where mass transfer at the interface is absent.

3 and 4 have no thermodynamic connections as they are just linked by mechanical equilibrium through a simple contact discontinuity. Consequently, the present test problem corresponds to a Riemann problem for a material with a phase transition and an equilibrium equation of state. Because of the discontinuity in the sound speed at the phase boundary, a rarefaction wave splits into two waves, due to the convex kink in the isentrope in the (p, v)-plane. This behaviour is well known. An extensive description of the Riemann problem for materials with phase transition can be found in Muller & Voss (2006).

A simple interpretation of the differences between the results of figure 10 where mass transfer is present and the results of figure 9 where mass transfer is absent can be obtained graphically in the (u, p)-plane. In both cases, the velocity and pressure in the shock state correspond to the intersection of the wave curves. The shock curve has a slope given by $\rho(D - u)$ where D represents the shock speed. The expansion wave has a slope given by $-\rho c$, where ρ represents the mixture density and c the mixture sound speed. For both cases (with and without mass transfer) the right-facing shock curve for the gas is the same, but the slope of the expansion wave varies when mass transfer occurs. Indeed, the left-facing wave curves for the liquid are the same until the rarefaction hits the phase boundary. The slope of this curve then changes drastically when mass transfer occurs, as the equilibrium sound speed is lower than the frozen one. Hence the intersection of the wave curves has larger value for u. This is clearly visible on these two figures where the velocity changes from 150 m s^{-1} up to 330 m s^{-1}.

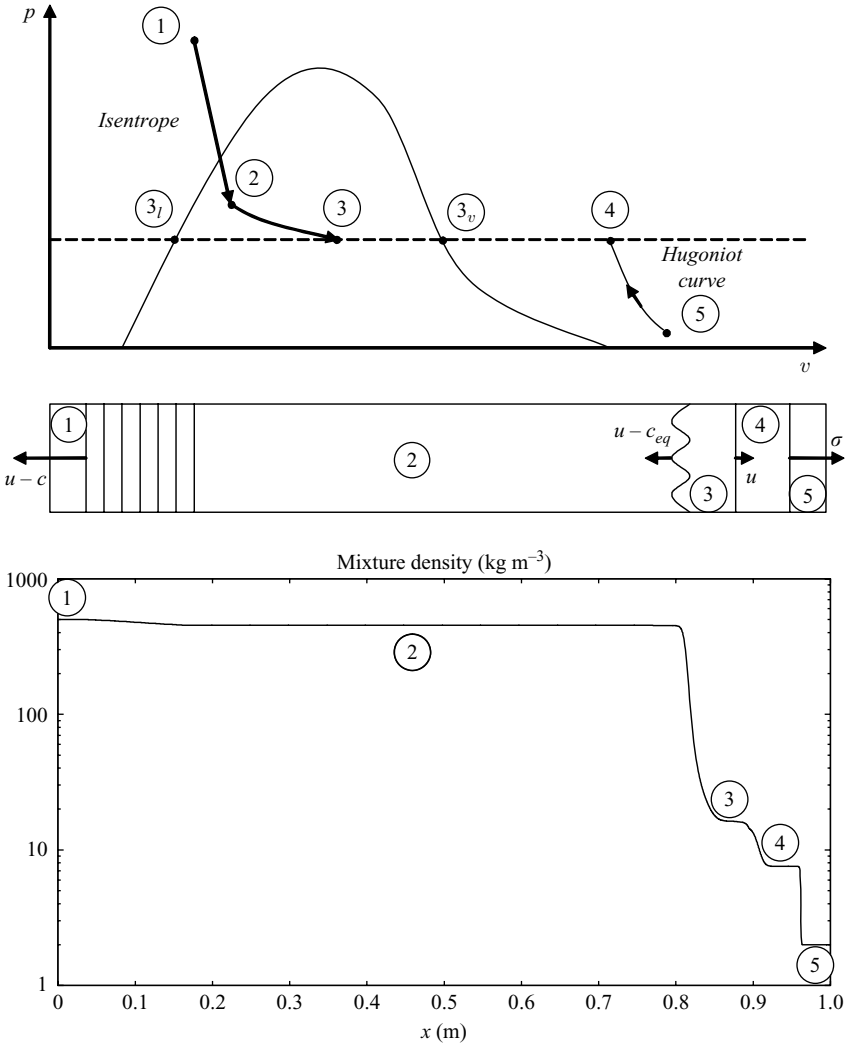

FIGURE 11. Phase-space trajectory for the flow simulated in figure 10. Trajectory between points 2 and 3 in the phase diagram represents kinetic connection between superheated liquid and equilibrium mixture. Points 3 and 4 have no thermodynamic connections as they are just linked by mechanical equilibrium through a simple contact discontinuity separating vaporized mixture and shocked initial vapour.

7.3. *Validation against shock tube experiments*

Experiments in shock tubes have been carried out by Simoes-Moreira & Shepherd (1999). Liquid dodecane is initially kept stable at a certain temperature and is suddenly expanded into a low-pressure chamber. An evaporation front propagates into metastable liquid dodecane ejecting high-velocity liquid–vapour mixture. The velocity of this front was measured for different initial temperatures of liquid dodecane. Front velocities are computed under the same conditions as the present model and compared with experiments. Results are shown in figure 12. Each point corresponds to a shock tube computation with a given initial temperature of the liquid in the high-pressure chamber. The agreement is not perfect but front velocities are of

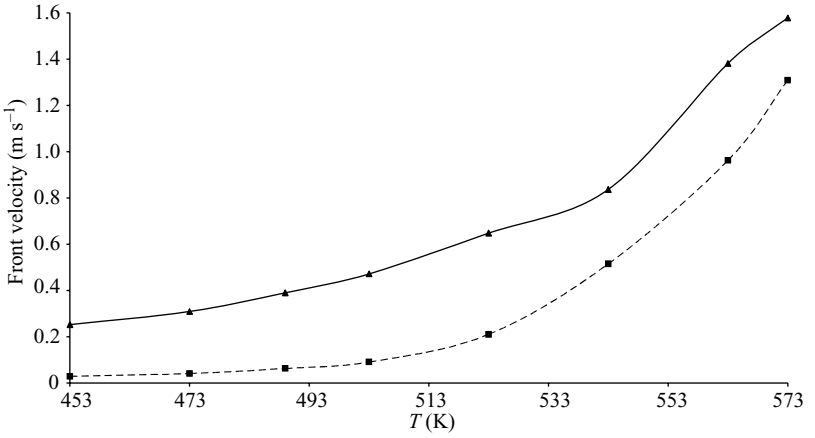

FIGURE 12. Evaporation front velocity in superheated dodecane versus initial temperature of liquid dodecane. The experimental results of Simoes-Moreira & Shepherd (1999) (solid line) are compared with front velocities computed with the new model (dashed line).

the same order of magnitude and the same tendency of increasing front velocity with increasing temperature is observed. The discrepancies between experimental and computed results are explained by the inaccuracies present in the simplified model EOS used for the phases. Using a more sophisticated EOS than SG (MG for example) is an option to improve this point (see the discussion in §4).

7.4. *The CJ kinetic relation*

The Chapman–Jouguet (CJ) kinetic relation is often used to close the Rankine Hugoniot system to deal with evaporation fronts in metastable liquids. In this context, the front is considered as a discontinuity whose speed is determined by the CJ condition. Obviously, such a procedure is approximate and valid only in limit situations, when the liquid is highly metastable so that the system tends to evaporate as fast as possible, i.e. with the maximum admissible mass flow rate. This limit evaporation regime is considered in the present model with a slight modification.

In the present model the interface is solved as a relaxation zone where the multiphase flow model tends to the equilibrium Euler equations. This last system admits very different waves speeds than the ones of the temperature non-equilibrium model. This results in the appearance of a transition front that corresponds to an expansion wave of the equilibrium model. Observation of the numerical results at different times shows a smearing of the evaporation wave, exactly as a computed expansion wave and not as a contact discontinuity. As represented in figure 13, this expansion wave propagates to the left at velocity approximately equal to $u - c_{eq}$. There is no contradiction up to this point between our modelling and previous Hugoniot analysis. Conventional modelling based on jump conditions closed by the CJ assumption consider the front as a discontinuity obeying the principle of mass, momentum and energy conservation with an evaporation wave propagating at the maximum admissible speed (CJ). Such a model was proposed by Chaves (1984) and validated against many experiments when a retrograde liquid is highly metastable. In our approach, the wave is solved as an expansion wave of the relaxed system. It also obeys to the principles of mass, momentum and energy conservation. Its speed corresponds to that of acoustic waves of the equilibrium system $u - c_{eq}$ with the sound speed given by (5.20). It is also associated with a pressure decrease, as in all

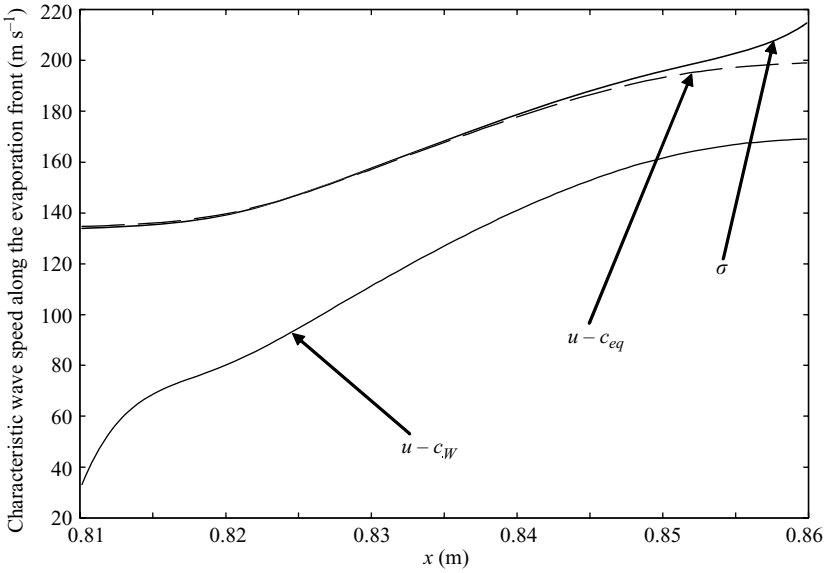

FIGURE 13. Comparison between local wave speed (solid lines) computed with $\sigma_i = (\rho u)_i - (\rho u)_{i-1}/(\rho_i - \rho_{i-1})$, characteristic velocity based on the equilibrium speed of sound $u - c_{eq}$ (dashed lines) and characteristic velocity based on the mechanical equilibrium $u - c_W$ (Wood) speed of sound. The comparison is for the flow simulated in figure 10 in the x-range where the evaporation front is present. It appears clearly that the evaporation front propagates at the local characteristic wave speed of the equilibrium system.

expansions waves. It is thus in agreement with the CJ representation, except that the front is not considered as a discontinuity.

Another difference appears regarding thermodynamics. The CJ state is a local entropy maximum on the expansive branch of the Hugoniot locus. In the present model, each point of the evaporation front is at constant entropy as the front corresponds to an expansion wave of the equilibrium system. Consequently, both models give front speeds of the same order of magnitude but correspond to different representations.

The differences in accuracy when compared for example with Simoes-Moreira & Shepherd's (1999) results are due to the EOS. The equilibrium EOS of the present relaxed system is not exactly the same as in Simoes-Moreira & Shepherd (1999). This is due to our non-equilibrium modelling where initially two EOS are used, resulting in an approximate equilibrium EOS.

Note that CJ evaporation fronts are associated with extreme conditions. Under moderate conditions, the front is subsonic and its dynamics is governed by multi-dimensional effects where thermal diffusion, capillary effects and chemical relaxation play an important role. Such effects can be introduced in the present approach by coupling the present relaxation method with the capillary and dissipative effects modelling described in Perigaud & Saurel (2005). Extra efforts are necessary to reach this goal.

7.5. *Two-phase expansion tube*

In the following examples, front propagation in pure liquids is not considered. The aim is now to deal with cavitation in liquids considered as not pure. Consequently the only evaporation criterion used to activate the phase transition process corresponds

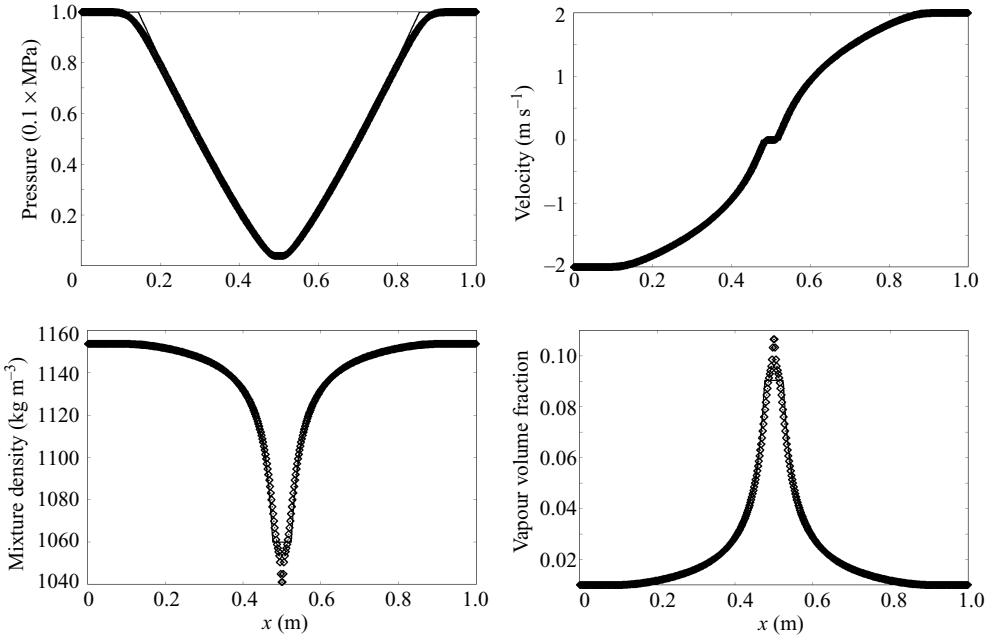

FIGURE 14. The multiphase model computed solution (symbols) without mass transfer is compared to the exact one (lines) for the symmetric expansion tube.

to the metastability criterion. Phase transition is allowed only if one of the fluids is metastable ($T_k > T_{\text{stat}}(P)$).

In this example, a 1 m long tube is filled with liquid water at atmospheric pressure and with density $\rho = 1150\,\text{kg m}^{-3}$. An initial velocity discontinuity is located at $x = 0.5$ m. On the left, the velocity is set to $u = -2\,\text{m s}^{-1}$ and on the right, $u = 2\,\text{m s}^{-1}$. An initial weak volume fraction of vapour water ($\alpha_v = 10^{-2}$) is added to the liquid. Thermodynamic parameters of water are given in table 1. First, the numerical solution without mass transfer is compared to the exact one. The solution is represented in figure 14 at time $t = 3.2$ ms. It results in left- and right-facing rarefaction waves. The vapour volume fraction increases at the centre of the domain. This is due to the gas mechanical expansion present in small proportions. This effect tends to create new interfaces in the domain. The dynamic appearance of these interfaces is considered in the numerical resolution as well as in the exact solution, provided in Petitpas *et al.* (2007). The gas pocket that appears is not due to mass transfer, but to mechanical relaxation only (bubble growth).

However, these rarefaction waves make the liquid metastable and phase transition may occur. Figure 15 presents the solution when mass transfer is involved. The solution is shown at the same time as previously and compared to the previous exact solution without evaporation. Liquid water is expanded until the saturation pressure is reached (see the pressure graph) then evaporation appears and a quite small amount of vapour is created (see the mass fraction graph). This small amount of vapour has nevertheless large consequences for the vapour volume fraction that increases significantly.

The solution with mass transfer is composed of four expansion waves, as shown in figure 16. In order to highlight the two slow expansion waves, the solution is shown at time $t = 59$ ms in figure 17. The two leading fast expansion waves have left

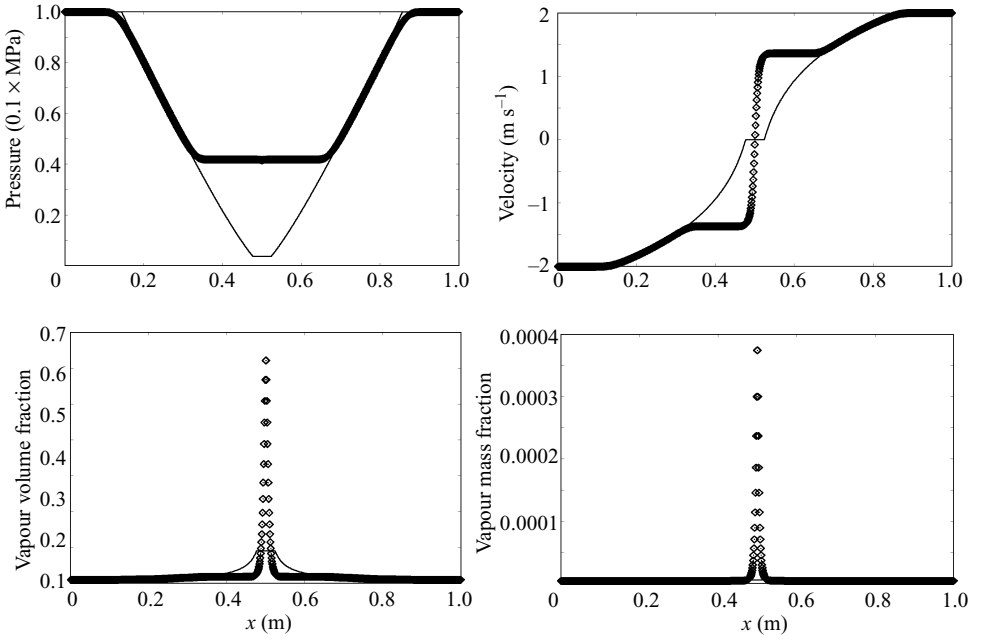

FIGURE 15. The multiphase model computed solution (symbols) with mass transfer is compared to the exact one (lines) without mass transfer for the symmetric expansion tube. Mass transfer appears and results in important differences for all flow variables.

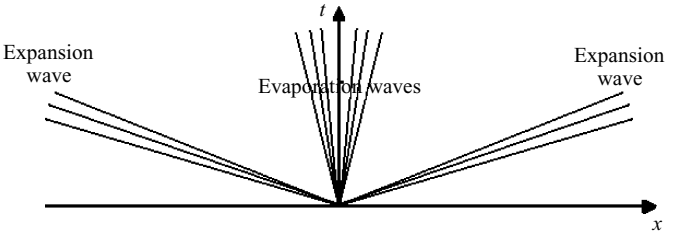

FIGURE 16. Wave propagation diagram of the symmetric expansion tube.

the tube. The two slow evaporation fronts have characteristic profiles of expansion waves. This observation confirms the previous interpretation of evaporation fronts as expansion waves of the equilibrium system. When rarefaction effects become stronger, it is possible to see the four waves present on a single graph. In figure 18 the same conditions are used except regarding velocities which are set to $u = -500$ m s^{-1} on the left, and $u = 500$ m s^{-1} on the right. In this case, evaporation is much more intense resulting in a large cavitation pocket where the gas volume fraction is close to 1. However, this pocket does not contain pure gas but a mixture at thermodynamic equilibrium as shown on the mass fraction profile. The various expansion waves now have comparable velocities, as shown in figure 19.

7.6. *Two-dimensional illustrations*

The model capabilities are now illustrated for severe test problems involving cavitation pockets with or without evaporation. The first example is related to supercavitation

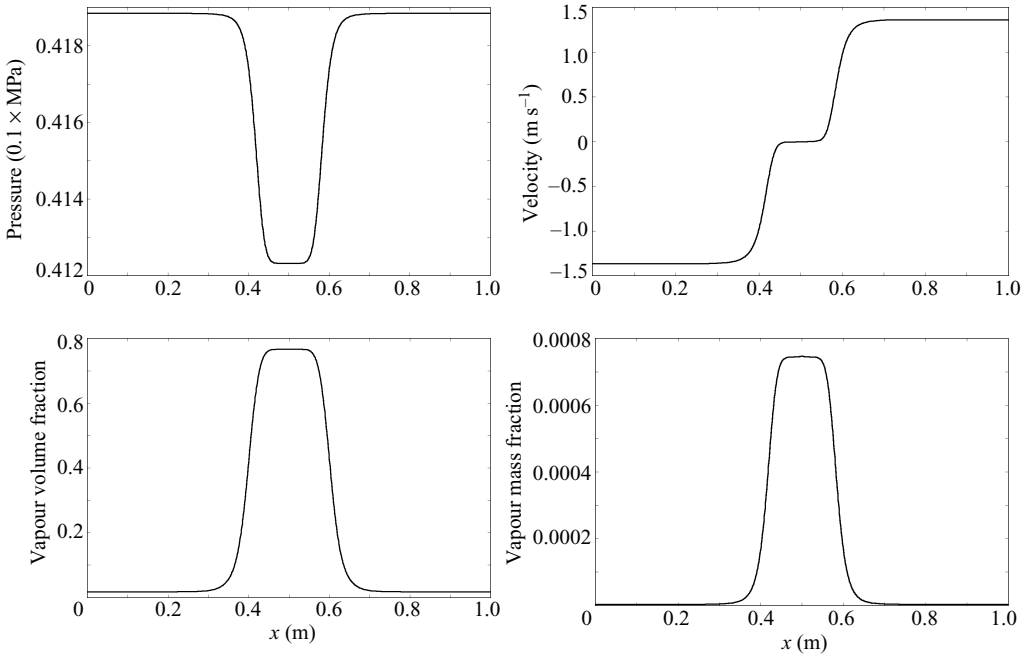

FIGURE 17. Long time behaviour for the test problem of figure 15. The two slow expansion waves are clearly visible.

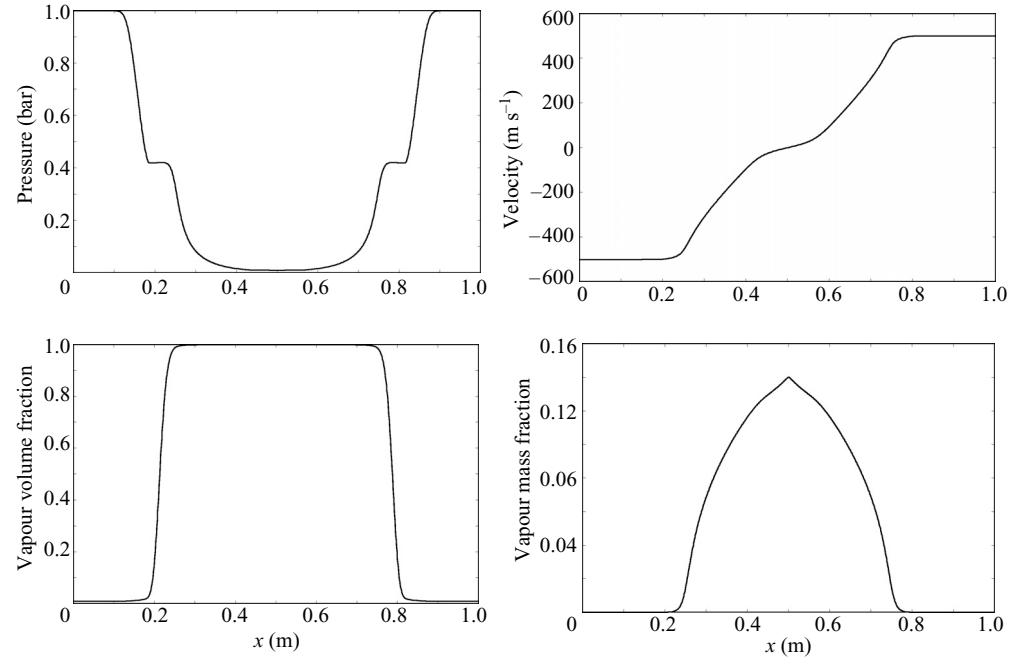

FIGURE 18. Numerical solution of the multiphase flow model with mass transfer and strong velocity difference in the expansion tube. The four expansion waves are clearly visible.

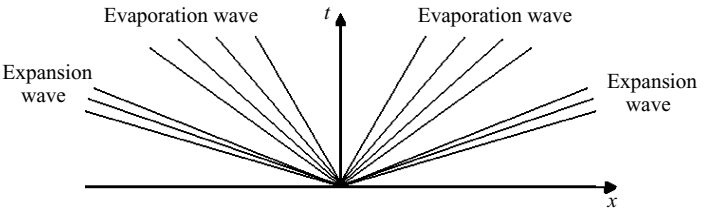

FIGURE 19. Schematic (x, t) diagram of the strong symmetric expansion tube.

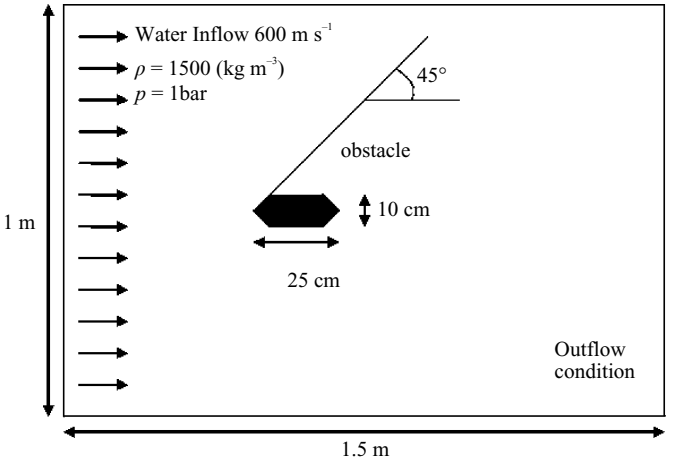

FIGURE 20. Initial configuration of a high-velocity underwater projectile.

around a high-velocity underwater projectile. The second test is related to cavitation pockets in fuel injector nozzles.

7.6.1. *High-velocity underwater projectile*

A liquid water flow at velocity 600 m s^{-1} around an immersed obstacle is considered as shown in figure 20. Liquid water is initially at atmospheric pressure with a density of 1150 kg m^{-3}. A weak volume fraction of vapour ($\alpha_v = 10^{-3}$) is initially present in the water. At the leading edge of the obstacle a strong compression zone is present and the pressure exceeds 2000 atm. Then the high-velocity liquid flow is subject to strong rarefaction waves at each geometrical singularity and the pressure decreases.

On the left-hand side of figure 21 the computational results are shown at steady state without mass transfer. In the absence of mass transfer, the simulation does not break down as a small volume fraction of gas is present everywhere: the pressure, the volume fraction and the square speed of sound remain positive. This is a nice feature of the Kapila *et al.* (2001) model. This model however needs a specific numerical scheme as it is non-conservative. An appropriate numerical method is developed in Petitpas *et al.* (2007).

On the right-hand side of figure 21, mass transfer is involved. Qualitatively, both results are very similar: a cavitation wake appears. But the mechanisms responsible for these cavitation waves are very different. On the left, only mechanical effects are responsible for bubble growth while on the right mechanical and chemical relaxation effects are responsible for the pocket growth. This means that results without mass

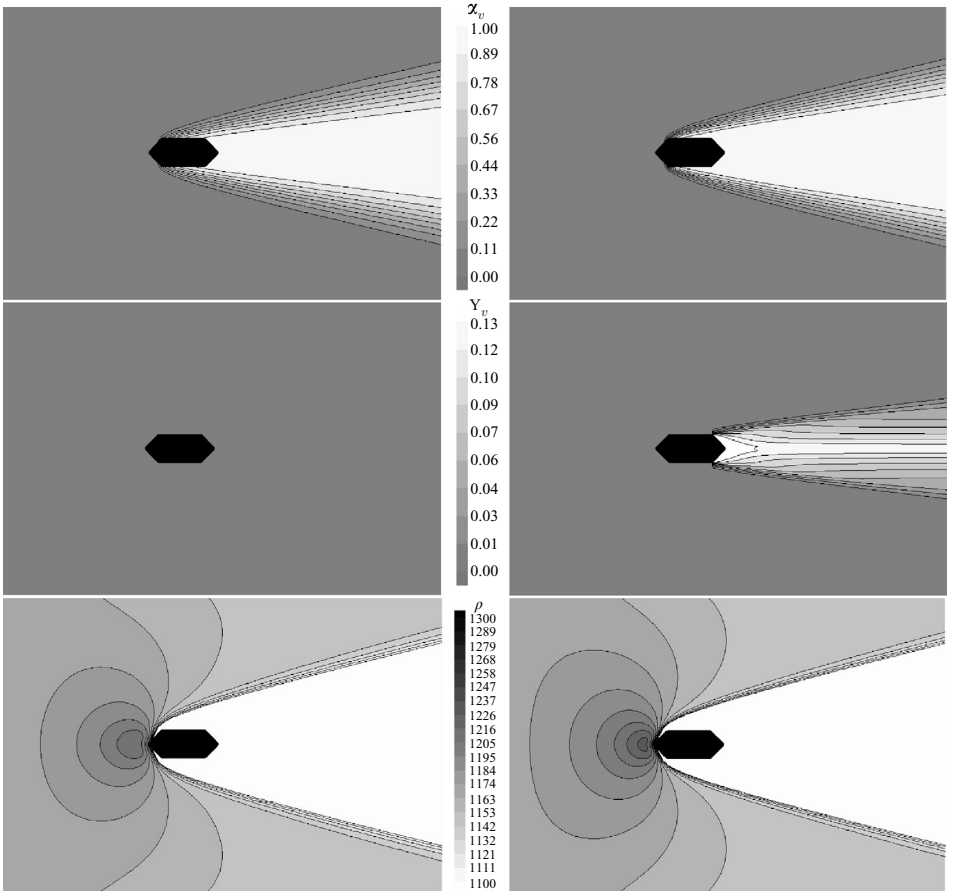

FIGURE 21. High-velocity underwater projectile. On the left, the solution obtained without heat and mass transfer and on the right the solution with the new thermo-chemical solver. Solutions are shown at steady state. From top to bottom, contours of: vapour volume fraction, vapour mass fraction and mixture density. White regions represent from top to bottom respectively: regions where vapour volume fraction is close to 1, regions where vapour mass fraction becomes non-negligible (0.1) and regions where mixture density is lower than the density at infinity.

transfer can be used for a qualitative prediction of the locations where cavitation appears. For a quantitative prediction, results with mass transfer are more realistic. It is interesting to note that the maximum vapour mass fraction is not very large (less than 0.13). The pressure level in the cavitation pocket is quite different: 0.4 atm with mass transfer, corresponding to the saturation pressure, to be compared with 10^{-3} atm in the absence of mass transfer.

7.6.2. *High-pressure fuel injector*

The second situation under study consists of a nozzle where liquid fuel, from a high-pressure chamber is injected into another chamber at atmospheric pressure as shown in figure 22. The high-pressure tank (1000 atm) is filled with liquid dodecane at density $570\,\mathrm{kg\,m^{-3}}$, corresponding to the temperature $T = 640$ K (lower than the critical temperature). As previously a weak volume fraction of vapour ($\alpha_v = 10^{-4}$) is present in the liquid. The initial conditions consist of an initial discontinuity between

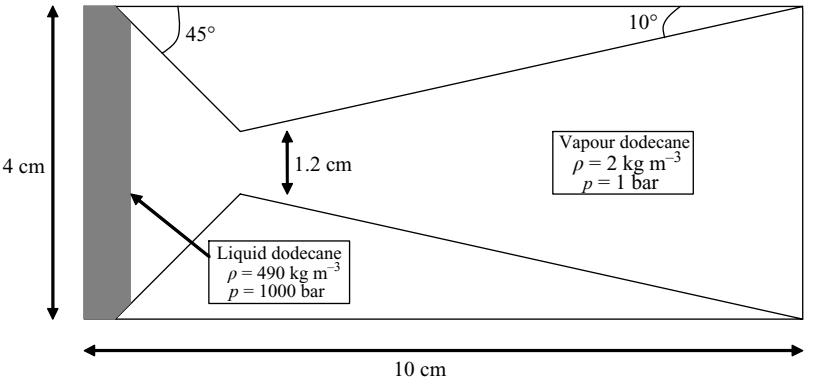

FIGURE 22. Initial configuration of a high-pressure fuel injector.

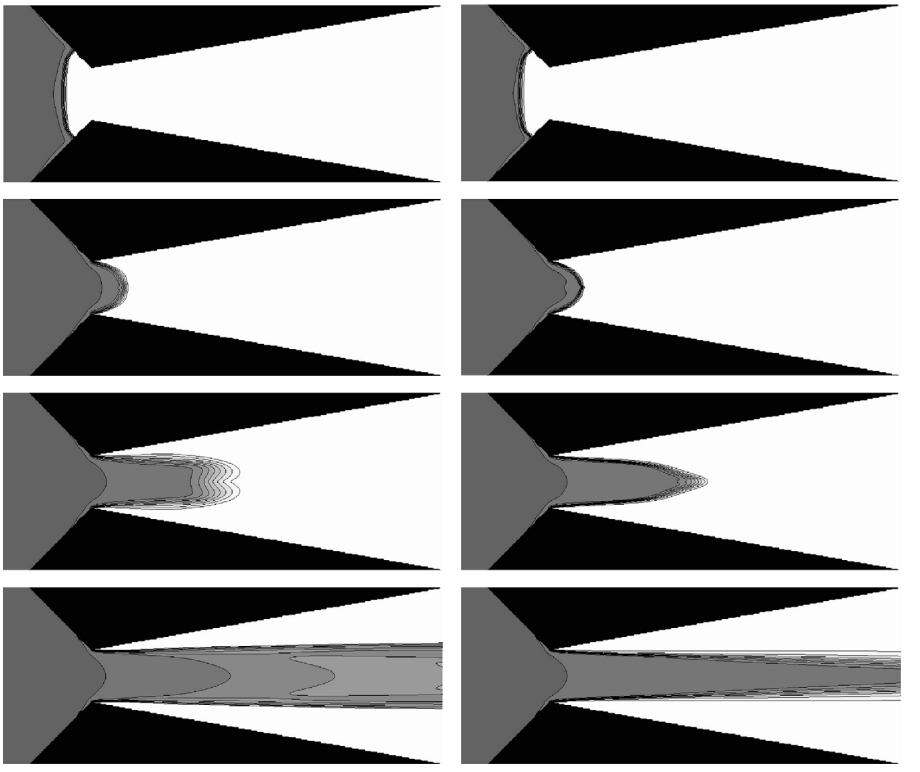

FIGURE 23. Flow in a high-pressure fuel injector. Mixture density contours are shown at times $t = 24$ μs, $t = 60$ μs, $t = 120$ μs and $t = 600$ μs. On the left, the solution is obtained without heat and mass transfers and on the right the solution is obtained with the thermo-chemical solver.

liquid dodecane at 1000 bar and 570 kg m^{-3} and its vapour at atmospheric pressure. Results are shown in figure 23 at times $t = 24$ μs, $t = 60$ μs, $t = 120$ μs, $t = 600$ μs. On the left, computed results without mass transfer are presented, and on the right those including evaporation. As in the preceding example, the results are qualitatively similar. But quantitative differences are present regarding flow variables.

It is interesting to note that only slight differences in cavitation pocket size are present. Two-phase nozzle flows have been used in the past to determine the mass

transfer rate in non-equilibrium two-phase flow models. The mass transfer rate was adjusted in order to match the cavitation pocket size. The present computations show that such a method is inappropriate. Indeed, cavitation pocket size has a too weak dependence on mass transfer. Mechanical effects alone are able to produce significant cavitation pockets.

8. Conclusions

A new hyperbolic compressible flow model has been constructed for the computation of cavitating flows. Relaxation effects are modelled and are able to connect the non-equilibrium flow model to the mixture Euler model when thermodynamic equilibrium is reached. The connection occurs through rarefaction waves where mass transfer occurs. The overall model is able to predict dynamic evaporation waves as well as interfaces of simple contact separating non-miscible phases.

The model gives a new interpretation of evaporation fronts (Chaves 1984) as expansion waves in the limit of stiff thermal and chemical relaxation. Numerical examples show that the model is able to predict complex flow pattern in one and two dimensions.

The authors are very grateful to anonymous referees for the time spent reading and analysing the manuscript. Many insightful remarks helped the authors to improve the quality of the paper. Part of this work was done while the first author was visiting the Institute for Mathematical Sciences, National University of Singapore in 2007. The visit was supported by the Institute and is gratefully acknowdledged.

Appendix A. Determination of equilibrium speed of sound

From the definition of mixture internal energy, we have

$$e = \left(\alpha_1\rho_1 e_1 + \alpha_2\rho_2 e_2\right)/\rho. \tag{A 1}$$

When the mixture evolves under thermodynamic equilibrium, the temperature is linked to the pressure (4.3). Each thermodynamic variable can thus be expressed as a function of pressure only: $e_k(p)$ and $\rho_k(p)$. Equation (A 1) can be written as

$$e(\rho, p) = \frac{1}{\rho}\left(\rho_1 e_1 + \frac{\rho - \rho_1}{\rho_2 - \rho_1}(\rho_2 e_2 - \rho_1 e_1)\right). \tag{A 2}$$

The mixture speed of sound is defined as

$$c^2 = \left(\frac{\partial p}{\partial \rho}\right)_s = \frac{\dfrac{p}{\rho^2} - \left(\dfrac{\partial e}{\partial \rho}\right)_p}{\left(\dfrac{\partial e}{\partial p}\right)_\rho}. \tag{A 3}$$

Differentiating e with respect to ρ and p, we obtain

$$\frac{1}{\rho c_{eq}^2} = \frac{-\dfrac{\mathrm{d}\rho_1}{\mathrm{d}p}\alpha_1\rho_2\left(\dfrac{e_2 - e_1}{\rho_2 - \rho_1}\right) - \dfrac{\mathrm{d}\rho_2}{\mathrm{d}p}\alpha_2\rho_1\left(\dfrac{e_2 - e_1}{\rho_2 - \rho_1}\right) + \dfrac{\mathrm{d}e_1}{\mathrm{d}p}\alpha_1\rho_1 + \dfrac{\mathrm{d}e_2}{\mathrm{d}p}\alpha_2\rho_2}{p - \rho_1\rho_2\left(\dfrac{e_2 - e_1}{\rho_2 - \rho_1}\right)}. \tag{A 4}$$

This sound speed is the equilibrium one as (4.3) has been used. We now use the Gibbs relation for each phase:

$$\forall k = 1, 2: \qquad \frac{\mathrm{d}e_k}{\mathrm{d}p} = T\frac{\mathrm{d}s_k}{\mathrm{d}p} + \frac{p}{\rho_k^2}\frac{\mathrm{d}\rho_k}{\mathrm{d}p}. \tag{A 5}$$

Noting that

$$\text{for } k = 1, 2: \qquad \frac{\mathrm{d}\rho_k}{\mathrm{d}p} = \left(\frac{\partial\rho_k}{\partial p}\right)_{s_k} + \left(\frac{\partial\rho_k}{\partial s_k}\right)_p \frac{\mathrm{d}s_k}{\mathrm{d}p}, \tag{A 6}$$

we obtain the mixture equilibrium speed of sound formulation (5.20):

$$\frac{1}{\rho c_{eq}^2} = \frac{\alpha_1}{\rho_1 c_1^2} + \frac{\alpha_2}{\rho_2 c_2^2} + T\left[\frac{\alpha_1\rho_1}{C_{p,v}}\left(\frac{\mathrm{d}s_1}{\mathrm{d}p}\right)^2 + \frac{\alpha_2\rho_2}{C_{p,l}}\left(\frac{\mathrm{d}s_2}{\mathrm{d}p}\right)^2\right].$$

Appendix B. Coefficients A, B, A' and B' for thermo-chemical solver

In order to determine heat and mass transfer terms (6.6), the four coefficients A, B, A' and B' have to be calculated at time t^n. Here, we provide expressions for these coefficients in the context of SG EOS:

$$\begin{aligned}
A &= -(C_1 - C_2)\rho c^2\left(\frac{\Gamma_1}{\rho_1 c_1^2} - \frac{\Gamma_2}{\rho_2 c_2^2}\right) + \frac{1}{C_{v,1}\gamma_1\alpha_1\rho_1} + \frac{1}{C_{v,2}\gamma_2\alpha_2\rho_2},\\
B &= -(C_1 - C_2)\rho\left[\left(\frac{\rho c^2}{\rho_1} - \Gamma h_1\right) - \left(\frac{\rho c^2}{\rho_2} - \Gamma h_2\right)\right]\\
&\quad - \rho\Gamma(h_1 - h_2)\left(\frac{1}{C_{v,1}\gamma_1\Gamma_1\rho_1} - \frac{1}{C_{v,2}\gamma_2\Gamma_2\rho_2}\right),\\
A' &= (D_1C_1 - D_2C_2)\rho c^2\left(\frac{\Gamma_1}{\rho_1 c_1^2} - \frac{\Gamma_2}{\rho_2 c_2^2}\right)\\
&\quad - \left(1 + \frac{D_1}{C_{v,1}\gamma_1}\right)\frac{1}{\alpha_1\rho_1} - \left(1 + \frac{D_2}{C_{v,2}\gamma_2}\right)\frac{1}{\alpha_2\rho_2},\\
B' &= (D_1C_1 - D_2C_2)\rho\left[\left(\frac{\rho c^2}{\rho_1} - \Gamma h_1\right) - \left(\frac{\rho c^2}{\rho_2} - \Gamma h_2\right)\right]\\
&\quad + \rho\Gamma(h_1 - h_2)\left[\left(1 + \frac{D_1}{C_{v,1}\gamma_1}\right)\frac{1}{\Gamma_1\rho_1} + \left(1 + \frac{D_2}{C_{v,2}\gamma_2}\right)\frac{1}{\Gamma_2\rho_2}\right],
\end{aligned}$$

where the coefficients C_k and D_k are given for each phase k by

$$C_k = \frac{(1 - \gamma_k T_k)}{\gamma_k(p + p_{\infty,k})}, \quad D_k = \frac{q_k - g_k}{T_k}.$$

REFERENCES

Abgrall, R. & Saurel, R. 2003 Discrete equations for physical and numerical compressible multiphase mixtures. *J. Comput. Phys.* **186**, 361–396.

Baer, M. R. & Nunziato, J. W. 1986 A two-phase mixture theory for the deflagration-to-detonation transition (DDT) in reactive granular materials. *Intl J. Multiphase Flows* **12**, 861–889.

Butler, P. B., Lambeck, M. F. & Krier, H. 1982 Modeling of shock development and transition to detonation initiated by burning in porous propellant beds. *Combust. Flame* **46**, 75–93.

Cahn, J. W. & Hilliard, J. E. 1958 Free energy of a nonuniform system i: Interfacial free energy. *J. Chem. Phys.* **28**, 258–267.

Chaves, H. 1984 Changes of phase and waves on depressurization of liquids with high specific heat. Ph D thesis, Georg-August-Universitat, Gottingen.

Chinnayya, A., Daniel, E. & Saurel, R. 2004 Computation od detonation waves in heterogeneous energetic materials. *J. Comput. Phys.* **196**, 490–538.

Delhaye, J. M. & Boure, J. A. 1982 General equations and two-phase flow modeling. In *Handbook of Multiphase Systems* (ed. G. Hestroni), Hemisphere.

Faucher, E., Herard, J. M., Barret, M. & Toulemonde, C. 2000 Computation of flashing flows in variable cross section ducts. *Intl J. Comput. Fluid Dyn.* **13**, 365–391.

Frost, D. L., Lee, J. H. S. & Ciccarelli, G. 1991 The use of hugoniot analysis for the propagation of vapor explosion waves. *Shock Waves* **1**, 99–110.

Grolmes, M. A. & Fauske, H. K. 1974 Axial propagation of free surface boiling into superheated liquids in vertical tubes. *Heat Transfer* **4**, 30–34.

Hill, L. G. & Sturtevant, B. 1990 An experimental study of evaporation waves in a superheated liquid. In *Adiabatic Waves in Liquid-Vapor Systems* (ed. G. E. A. Meier & P. A. Thompson), pp. 25–37. Springer.

Ishii, M. 1975 *Thermo-Fluid Dynamic Theory of Two-Phase Flow*. Eyrolles, Paris.

Jamet, D., Lebaigue, O., Coutris, N. & Delhaye, J. M. 2001 The second gradient method for the direct numerical simulation of liquid-vapor flows with phase change. *J. Comput. Phys.* **169**, 624–651.

Kapila, A., Menikoff, R., Bdzil, J., Son, S. & Stewart, D. 2001 Two-phase modeling of DDT in granular materials: reduced equations. *Phys. Fluids* **13**, 3002–3024.

Kurschat, Th., Chaves, H. & Meier, G. E. A. 1992 Complete adiabatic evaporation of highly superheated liquid jets. *J. Fluid Mech.* **236**, 43–59.

Le Metayer, O., Massoni, J. & Saurel, R. 2004 Elaborating equations of state of a liquid and its vapor for two-phase flow models. *Intl J. Therm. Sci.* **43**, 265–276.

Le Metayer, O., Massoni, J. & Saurel, R. 2005 Modeling evaporation fronts with reactive Riemann solvers. *J. Comput. Phys.* **205**, 567–610.

Liou, M. S. & Edwards, J. R. 1999 AUSM schemes and extensions for low Mach and multiphase flows. *30th Computational Fluid Dynamics Conf., March 8-12*. Lecture Series 1999-03, Von Karman Institute for Fluid Dynamics.

Menikoff, R. & Plohr, B. J. 1989 The Riemann problem for fluid flow of real materials. *Rev. Mod. Phys.* **61**, 75–130.

Muller, S. & Voss, A. 2006 The riemann problem for the Euler equations with nonconvex and nonsmooth equations of state: Construction of the waves curves. *SIAM J. Sci. Comput.* **28**, 651–681.

Murrone, A. & Guillard, H. 2004 A five equations reduced model for compressible two-phase flow problems. *J. Comput. Phys.* **202**, 664–698.

Oldenbourg, R. 1989 *Properties of Water and Steam in SI-units*. Springer.

Perigaud, G. & Saurel, R. 2005 A compressible flow model with capillary effects. *J. Comput. Phys.* **209**, 139–178.

Petitpas, F., Franquet, E., Saurel, R. & Le Metayer, O. 2007 A relaxation-projection method for compressible flows. Part 2: Artificial heat exchange for multiphase shocks. *J. Comput. Phys.* **225**, 2214–2248.

Reinke, P. & Yadigaroglu, G. 2001 Explosive vaporization of superheated liquids by boiling fronts. *Intl J. Multiphase Flows* **27**, 1487–1516.

Saurel, R. & Abgrall, R. 1999 A multiphase Godunov method for compressible multifluid and multiphase flows. *J. Comput. Phys.* **150**, 425–467.

Saurel, R., Cocchi, J. P. & Butler, P. B. 1999 A numerical study of cavitation in the wake of a hypervelocity underwater projectile. *J. Propulsion Power* **15**, 513–522.

Saurel, R., Franquet, E., Daniel, E. & Le Metayer, O. 2007*a* A relaxation-projection method for compressible flows. Part 1: The numerical equation of state for the Euler Equations. *J. Comput. Phys.* **223**, 822–845.

Saurel, R., Gavrilyuk, S. & Renaud, F. 2003 A multiphase model with internal degrees of freedom: application to shock-bubble interaction. *J. Fluid Mech.* **495**, 283–321.

Saurel, R. & Le Metayer, O. 2001 A multiphase model for compressible flows with interfaces, shocks, detonation waves and cavitation. *J. Fluid Mech.* **431**, 239–271.

Saurel, R., Le Metayer, O., Massoni, J. & Gavrilyuk, S. 2007*b* Shock jump relations for multiphase mixtures with stiff mechanical relaxation. *Shock Waves* **16**, 209–232.

Simoes-Moreira, J. R. 1994 Adiabatic evaporation waves. PhD Thesis, Rensselaer Polytechnic Institute, Troy.

Simoes-Moreira, J. R. & Shepherd, J. E. 1999 Evaporation waves in superheated dodecane. *J. Fluid Mech.* **382**, 63–86.

Thompson, P. A., Chaves, H., Meier, G. E. A, Kim, Y. G. & Speckmann, H. D. 1987 Wave splitting in a fluid of large heat capacity. *J. Fluid Mech.* **185**, 385–414.

Wood, A. B. 1930 *A Textbook of Sound*. G. Bell and Sons Ltd, London.